548.732

THE PROBLEM OF IMAGE FORMATION IN X-RAY OPTICS

V. L. INDENBOM and F. N. CHUKHOVSKIĬ

Institute of Crystallography, USSR Academy of Sciences

Usp. Fiz. Nauk 107, 229–265 (June, 1972)

TABLE OF CONTENTS

1. INTRODUCTION

SINCE M. von Laue discovered x-ray diffraction, various methods of x-ray study of the structure and properties of crystals have been developed and have gained widespread practical application. Until recently, all these methods were based on the simplified so-called kinematical theory of scattering. The latter assumes that the regions of coherent scattering of x-rays in the crystal are so small that the primary x-ray beam is only slightly perturbed, and that we can neglect multiple scattering, interference of scattered beams, and attenuation of the primary beam. The successes of x-ray diffraction studies using the kinematical approximation in structural analysis,[1] in studying various crystal defects,[2] in determining internal stresses,[3] in studying electronic spectra by x-ray spectroscopic methods,[4] and in analyzing the thermal vibrations of atoms[5] have become firmly implanted in modern solid state physics and physical materials science.

Nevertheless, the bases of the dynamical theory were laid even in the first theoretical studies on x-ray diffraction.[6] This theory did not at all assume the crystal to be imperfect, but conversely, treated it as being ideal and possessing an absolutely regular lattice and serving as a resonator for the incident x-ray beam. Since the intensity of the coherently scattered beams is not considered small in comparison with the primary beam, all these beams in the dynamical theory are given equal weight, and the field in the crystal is found by solving the Maxwell equations for a system of self-consistent oscillating dipoles (the Ewald method). Alternatively and equivalently, they are solved for an inhomogeneous medium whose polarizability depends periodically on the coordinates (the Darwin method). The renewed interest of recent years in the dynamical theory of x-ray scattering has involved appearance of new ways of applying crystals in science and technology that require continually more perfect single crystals, and that have given rise to new methods of studying the quality of crystals. X-ray diffraction study has progressed from analyzing the shapes of lines in powder patterns or spots in Laue patterns to x-ray photographic methods that give an image of the internal structure of a crystal in a given Laue reflection with a resolution that makes it possible to reveal and identify individual dislocations.[7-9a]

New needs and new experimental potentialities have hastened the development of the dynamical theory of x-ray scattering. The effect of anomalous transmission of x-ray through a perfect crystal set in an exact Bragg position (the Borrmann effect[10a,11]) has been studied in detail. A theory of x-ray scattering has been developed that takes account of thermal vibrations of atoms.[12] In particular, the latter permits one to analyze inelastic diffuse scattering under conditions of dynamical scattering.[13] The problem of formation of a dynamical x-ray image of a crystal containing defects of various types has been studied intensively. Here the problem has proved to be especially complex, and the theory has lagged markedly behind experiment.

Various methods of x-ray topography have already become widespread in the practice of studying the actual structures of semiconductor, ionic, or metallic crystals. They are highly sensitive to defects in the ideality of the crystal structure, and they allow one to get information on the volume distribution of defects without harming the integrity and quality of the specimen. In particular, these methods have already been in use for several years in the semiconductor industry for factory control of perfection of crystals. However, the lack of a theory of formation of the image of an actual crystal leads to loss of the rich information obtained experimentally, and it puts x-ray topography at a disadvantage with respect to the optical and electron-microscopic methods of studying crystals. Further, it is the chief obstacle to effective application of x-ray topography in the practice of industrial and scientific laboratories.

Just as in interference optical microscopy[14] and diffraction electron microscopy,[15,16] the image in topograms arises from the phenomenon of phase contrast: the x-ray wave field in an inhomogeneous crystal proves to be spatially modulated in phase as well as in amplitude. The specifics of x-ray diffraction image formation, in contrast to optical and electron-microscopic image formation, is determined by the relation between the wavelength λ of the radiation and the interatomic distance d. While $\lambda \gg d$ in optics, and $\lambda \ll d$

in electron microscopy, $\lambda/d \lesssim 1$ for x-rays, and correspondingly, the diffraction angle proves to be of the order of unity. Consequently, not only regions of the crystal that extend in the direction of illumination participate in forming each detail of the x-ray image, but also those that extend in the perpendicular direction. While in electron microscopy the image can be considered to consist of points, each of which depicts the structure of the specimen along the direction of illumination (the columnar approximation [16]), in x-ray topography the image should rather be considered to be streaked, in that each point in the crystal corresponds to a strip having a length of the order of the specimen thickness. Overlap of the geometrical and diffraction images, which is rarely found in optics and electron microscopy, proves to be the general case in x-ray topography.

Various approaches have been proposed in recent years in the literature for solving the problem of x-ray image formation, the opportunity has arisen of analyzing the accumulated results and of planning methods of theoretical analysis of image formation that are very promising for practical use. This article will discuss a dynamical theory of formation of x-ray images that is based on representing the x-ray field in the form of two spatially-inhomogeneous wave packets. Chapter 2 will discuss a homogeneous wave field in an ideal crystal, as determining, in particular, the image of the surface relief and shape of the specimen. Chapter 3 will study an inhomogeneous wave field in an ideal crystal, and Green's functions will be constructed that describe the propagation of a local perturbation, and the images of slits, screens, and small volume inclusions will be analyzed. In Chap. 4, a general theory of image formation of a crystal having a known distortion field will be constructed, and special cases will be pointed out that allow simple analytical estimates. The results of numerical calculation of images of complex distortion fields caused by dislocations will be compared with approximate estimates obtained by using Green's functions. Chapter 5 will discuss geometrical x-ray optics. An analogy will be established between ray trajectories and the motion of charged particles in an electric field. Conditions will be derived for reflection and refraction of rays on passing through a phase boundary. Chapter 6 will develop a general method of constructing the analytic solution of the equations for the wave field in the crystal in the geometrical-optics approximation. As an example, the image of a dislocation perpendicular to the surface of the specimen will be constructed. The results will be compared with numerical calculation on a computer of the image of a dislocation and with experiment. An asymptotic method of image calculation is developed for a two-dimensional distortion field that simplifies analysis of the image for a thick crystal and that permits one directly to take account of effects of total internal reflection, waveguide formation, shadows, etc.

2. THE WAVE FIELD IN AN IDEAL CRYSTAL

We shall describe the x-ray field in the crystal by using the electric field vector $\mathbf{E}(\omega, \mathbf{r})$. This vector satisfies the Maxwell equation

$$\text{rot rot } \mathbf{E}(\omega, \mathbf{r}) = \varkappa^2 \varepsilon(\omega, \mathbf{r})\, \mathbf{E}(\omega, \mathbf{r}), \tag{2.1}$$

where $\varkappa$ and ω are the wave vector and frequency of the incident wave, and $\epsilon(\omega, \mathbf{r})$ is the dielectric constant. The latter differs little from unity, so that the polarizability of the crystal $\chi(\omega, \mathbf{r}) = \epsilon(\omega, \mathbf{r}) - 1$ is a small quantity.

In an ideal crystal, the function $\chi(\omega, \mathbf{r})$ depends periodically on the coordinates, and it can be expanded in a series in the reciprocal-lattice vectors $\mathbf{K}_h$:

$$\chi(\omega, \mathbf{r}) = \sum_h \chi_h(\omega)\, e^{i\mathbf{K}_h\mathbf{r}}. \tag{2.2}$$

The Bloch waves are solutions of Eq. (2.1):

$$\mathbf{E}_\mathbf{k}(\mathbf{r}) = e^{i\mathbf{k}\mathbf{r}} \sum_h \mathbf{E}_h e^{i\mathbf{K}_h\mathbf{r}}, \tag{2.3}$$

where the vector $\mathbf{k}$ satisfies the dispersion equation. The latter is obtained by substituting (2.3) into (2.1) and setting to zero the determinant of the matrix $A^{ij}_{hh'} = \{[(\mathbf{k}+\mathbf{K}_h)^2 - \varkappa^2]\delta_{ij}\delta_{hh'} - (\mathbf{k}+\mathbf{K}_h)_i(\mathbf{k}+\mathbf{K}_h)_j\delta_{hh'} - \varkappa^2\chi_{h-h'}\delta_{ij}\}$ that relates the components of the vectors $\mathbf{E}_h$.

a) The two-wave approximation. The case of greatest practical interest is that in which the crystal is oriented close to one of the Bragg positions, e.g., to a position having the reflection vector $\mathbf{K}_1$. Here one can restrict the expansion in (2.3) to two terms having amplitudes $\mathbf{E}_0$ and $\mathbf{E}_1$. The latter correspond to the transmitted and diffracted waves (the two-wave approximation):

$$\mathbf{E}_\mathbf{k} = \mathbf{e}_0 E_0 e^{i\mathbf{k}\mathbf{r}} + \mathbf{e}_1 E_1 e^{i\mathbf{k}_1\mathbf{r}}; \tag{2.4}$$

here $\mathbf{e}_0$ and $\mathbf{e}_1$ are unit vectors that are perpendicular to the vectors $\mathbf{k}$ and $\mathbf{k}_1 = \mathbf{k} + \mathbf{K}_1$, respectively (we can neglect the small departure of the electromagnetic field in the crystal from transverse orientation). They lie either in the scattering plane $\mathbf{k}, \mathbf{k}_1$ or perpendicular to it. The amplitudes E_0 and E_1 satisfy the following matrix equation arising from (2.1):

$$\begin{pmatrix} (k^2-\varkappa^2)\varkappa^{-2}-\chi_0 & -\chi_{-1}C \\ -\chi_1 C & (k_1^2-\varkappa^2)\varkappa^{-2}-\chi_0 \end{pmatrix} \begin{pmatrix} E_0 \\ E_1 \end{pmatrix} = 0, \tag{2.5}$$

where $C = 1$ for the components of the wave field polarized in the scattering plane, but $C = \cos 2\theta$ for the components polarized perpendicularly to this plane; $\theta = \widehat{\mathbf{k}\mathbf{k}_1}/2$ is the Bragg angle.

The dispersion equation corresponding to (2.5)

$$[(k^2 - \varkappa^2)\varkappa^{-2} - \chi_0]\,[(k_1^2 - \varkappa^2)\varkappa^{-2} - \chi_0] = C^2\chi_{-1}\chi_1$$

describes a surface of revolution with two branches having its axis parallel to the vector $\mathbf{K}_1$. Since we can treat the dispersion surface as an isoenergetic surface in reciprocal space, analysis of its shape differs in no way, e.g., from the usual analysis of the shape of a Fermi surface near the boundary of a Brillouin zone.

Figure 1 illustrates the cross section of the dispersion surface in the scattering plane. $\widetilde{OH} = \mathbf{K}_1$ is the reflection vector. The Bragg condition $k = k_1 = \varkappa$ ($OM = HM = \varkappa$) corresponds to point M, and the incident wave to point L. When the deviations from the Bragg conditions are large, the branches of the dispersion surface transform into the spheres T_0 and T_H having

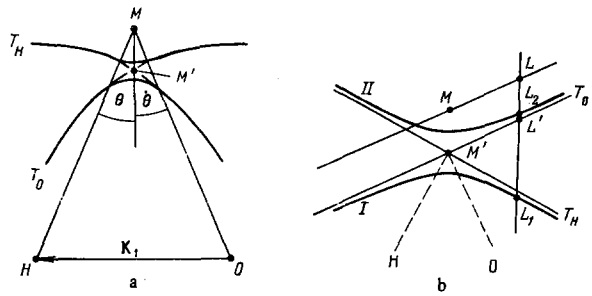

FIG. 1. Cross-section of the dispersion surface in the scattering plane.

centers at the points O and H (Fig. 1(a)), which are separated by the distance $\vec{OH} = \mathbf{K}_1$. When the deviation is small, they transform into hyperbolic cylinders (Fig. 1(b)). The radius of the spheres is $\kappa(1 + \chi_0)^{1/2}$. This corresponds to propagation of waves in a homogeneous medium having a refractive index of $(1 + \chi_0)^{1/2} \approx 1 + (\chi_0/2)$. (Since $\chi_0 < 0$, the crystal is a less dense medium than a vacuum for x-rays). The line of intersection of the spheres corresponds to point M'. Near this point, the spheres T_0 and T_H differ little from planes perpendicular to $\vec{OM'}$ and $\vec{HM'}$, and the dispersion surface is close to the hyperbolic cylinder

$$[\mathbf{k}\vec{M'O} - \kappa^2(1 + \chi_0)][\mathbf{k}_1\vec{M'H} - \kappa^2(1 + \chi_0)] = C^2\chi_{-1}\chi_1\kappa^2/4, \quad (2.6)$$

The planes T_0 and T_H serve as asymptotes for the latter (both χ_{-1} and χ_1 are negative, and hence the right-hand side of (2.6) is positive). The dispersion surface for polarization in the plane of incidence differs from that for polarization perpendicular to the plane in the greater length of the real axis of the hyperbola, which determines the minimum splitting of the dispersion surface

$$\Delta k_{\min} \approx \kappa C(\chi_{-1}\chi_1)^{1/2} \sec\theta. \quad (2.7)$$

When $\kappa \approx 10^8$ cm^{-1} and $|\chi| \approx 10^{-5}$, the splitting turns out to be of the order of 10^3 cm^{-1}.

b) Bloch functions. The different branches of the dispersion surface correspond to Bloch functions of different types. The first branch (the lower one in Fig. 19b)) corresponds to negative values of the two brackets on the left-hand side of Eq. (2.6). As we see from (2.5), $\mathbf{E}_0$ and $\mathbf{E}_1$ have the same sign in this case. Hence the antinodes of the Bloch functions pass near the lattice sites. The second (upper) branch of the dispersion surface corresponds to opposite signs for $\mathbf{E}_0$ and $\mathbf{E}_1$, and to antinodes of the Bloch functions lying between the lattice sites. In the symmetrical case (at the vertices of the hyperbolas), the vectors $\mathbf{E}_0$ and $\mathbf{E}_1$ are equal in absolute value, and the Bloch functions for polarization in the plane of incidence, when $\mathbf{e}_0 = \mathbf{e}_1$, take on the simple form

$$\mathbf{E}_k(\mathbf{r}) = 2\mathbf{e}_0E_0 \exp[i(\mathbf{k} + 0{,}5\mathbf{K}_1)\mathbf{r}] \cos(\mathbf{K}_1\mathbf{r}/2)$$

for the first branch, and

$$\mathbf{E}_k(\mathbf{r}) = -2i\mathbf{e}_0E_0 \exp[i(\mathbf{k} + 0{,}5\mathbf{K}_1)\mathbf{r}] \sin(\mathbf{K}_1\mathbf{r}/2) \quad (2.8)$$

for the second branch of the dispersion surface. In the former case, the nodes of the Bloch functions lie exactly between the lattice nodes. In the latter case, they lie in the reflecting atomic planes, and pass through the lattice nodes as the wave propagates. As we know, an analogous situation for the electronic wave functions occurs in the case of splitting of energy levels near the boundary of a Brillouin zone due to strong reflection of electrons.[17]

The noted difference between the Bloch functions proves to be very substantial when we take account of x-ray absorption. Photoelectric absorption gives rise to a small imaginary component in the polarizability $\chi(\omega, \mathbf{r})$. Correspondingly, the coefficients χ_h are complex quantities: $\chi_h' = \chi_h' + i\chi_h''$, where $0 < \chi_h'' < -\chi_h'$. The mean refractive index of the crystal $(1 + \chi_0)^{1/2} \approx 1 + (\chi_0'/2) + i(\chi_0''/2)$ corresponds to photoelectric absorption with an absorption coefficient $\mu = \kappa\chi_0''$. When $\chi_1' \approx \chi_{-1}'$, Eq. (2.6) gives the following expression for the absorption coefficient of the Bloch waves of the first type with $\mathbf{E}_0 \approx \mathbf{E}_1$:

$$\mu_1 = (\mu/\cos\theta)[1 + (C/2\chi_0'')(\chi_1'' + \chi_{-1}'')].$$

Analogously, for Bloch waves of the second type having $\mathbf{E}_0 \approx -\mathbf{E}_1$:

$$\mu_2 = (\mu/\cos\theta)[1 - (C/2\chi_0'')(\chi_1'' + \chi_{-1}'')]. \quad (2.9)$$

In both cases we have taken account of the fact that the direction of propagation of the studied Bloch waves forms the angles θ with the vectors $\mathbf{k}$ and $\mathbf{k}_1$. When $C = 1$ and $\chi_1'' \approx \chi_{-1}'' \approx \chi_0''$, we get $\mu_1 \approx 2\mu/\cos\theta$ and $\mu_2 \ll \mu_1$. That is, Bloch waves of the different types are absorbed to substantially different extents. Here the Bloch waves of the type of (2.8), which are polarized in the reflecting plane and which propagate along the reflecting planes in such a way that their nodes run along the atomic planes, show anomalously weak absorption as compared with the usual photoelectric absorption. This Borrmann[10a] effect of anomalous transmission of x-rays permits one to use perfect crystals as collimators with an angular divergence of the order of χ (i.e., of the order of several seconds of angle) and as polarizers with a degree of polarization of the order of $1 - \exp(-\delta\mu t)$. Here t is the thickness of the crystal, while $\delta\mu \approx \mu(1 - C)\sec\theta$ is the difference as defined by (2.9) between the minimum absorption coefficients for waves of differing polarization, which characterizes the x-ray dichroism of the crystal.

c) Excitation of the wave field in the crystal. In the general case, an external x-ray beam incident on a crystal excites in it an entire series of Bloch waves. Let a plane wave of wave vector κ ($\vec{LO}$ in Fig. 1) strike a plane face of a crystal set almost exactly at the Bragg position. Then, for each polarization, two Bloch waves having the wave vectors $\vec{L_1O}$ and $\vec{L_2O}$ in Fig. 1 are excited in the crystal. They correspond to two points L_1 and L_2 on the different branches of the dispersion surface that are related to the point L by the condition of continuity of the tangential component of the wave vector: at the surface of the crystal:

$$[\kappa\mathbf{n}] = [\mathbf{k}^{(\mathrm{I})}\mathbf{n}] = [\mathbf{k}^{(\mathrm{II})}\mathbf{n}], \quad (2.10)^*$$

Here $\mathbf{n}$ is the normal to the entrance surface of the

*$[\kappa n] \equiv \kappa \times n$.

crystal. The condition (2.10) implies that the points L, L_1, and L_2, which are the ends of the wave vectors $\kappa = \vec{LO}$, $k^{(I)} = \vec{L_1O}$, and $k^{(II)} = \vec{L_2O}$, lie on a single line parallel to the vector n (see Fig. 1). The intersection L′ of this plane with the asymptote T_0 defines the wave vector $\vec{L'O}$ (where $|\vec{L'O}| = \kappa' = (1 + \chi_0)^{1/2}$) for the wave that would have propagated in a crystal having the homogeneous polarizability $\chi = \chi_0$.

The Bloch waves having the similar wave vectors $k^{(I)}$ and $k^{(II)}$ propagate independently in the crystal. Their superposition results in an overall wave field that beats spatially with the wave vector $\Delta k = 0.5(k^{(I)} - k^{(II)})$ (the Pendellösung,[18a] which is analogous to the case of coupled pendulums in mechanics). Energy transfer from the transmitted to the diffracted wave, and vice versa, occurs within the distance $l = \pi/|\Delta k|$ in the direction normal to the entrance face. In the exact Bragg position, which corresponds to the minimum distance (2.7) between the branches of the dispersion surface, the distance l attains its maximum value $\Lambda = 2\pi(C\kappa)^{-1}(\chi_1\chi_{-1})^{1/2}\cos\theta$, which is called the extinction distance. According to (2.5), the relation between the amplitudes E_0 and E_1 in each of the Bloch waves is defined by the proportion

$$E_0/E_1 = C\chi_{-1}/|(k^2 - \varkappa^2)\varkappa^{-2} - \chi_0|. \qquad (2.11)$$

Apart from correction factors of the order of χ_0 (i.e., neglecting corrections for the mean refraction), the amplitudes of the Bloch functions can be found from the condition of continuity of the electromagnetic field at the surface of the crystal: the sum of the Bloch waves of (2.4) for the vectors $k^{(I)}$ and $k^{(II)}$ (and for both polarizations) must give values at the entrance face for the electric field strength and its normal gradient that match the field of the wave incident on the crystal.

A number of monographs and reviews[18b] give the detailed solution of the boundary problems in the dynamical theory of scattering of plane waves. We shall give as an example only the expression for the overall wave field polarized in the scattering plane for the case $n \cdot K_1 = 0$ (symmetric Laue diffraction):

$$E(r) = e_0E_0(z)\,e^{i\varkappa r} + e_1E_1(z)\,e^{i(\varkappa+K_1)r}, \qquad (2.12)$$

where

$$E_0(z) = \exp\{i[(\chi_0\varkappa z/2\cos\theta) - (\alpha\varkappa z/4\cos\theta)]\}\{\cos[(\chi_1\varkappa z/2\cos\theta)[1 + (\alpha/2\chi_1)^2]^{1/2}] + (i\alpha/2\chi_1)\sin[(\chi_1\varkappa z/2\cos\theta)[1 + (\alpha/2\chi_1)^2]^{1/2}][1 + (\alpha/2\chi_1)^2]^{-1/2}\}, \qquad (2.13)$$

$$E_1(z) = i\exp\{i[(\chi_0\varkappa z/2\cos\theta) - (\alpha\varkappa z/4\cos\theta)]\} \times \sin\{(\chi_1\varkappa z/2\cos\theta)[1 + (\alpha/2\chi_1)^2]^{1/2}\}[1 + (\alpha/2\chi_1)^2]^{-1/2}; \qquad (2.14)$$

Here $z = r \cdot n$ is the distance from the entrance face of the crystal, we have assumed for simplicity that $\chi_1 = \chi_{-1}$ (which is valid for a centrosymmetric crystal), and the parameter $\alpha = [(\kappa + K_1)^2 - \kappa^2]/\kappa^2$ is determined by the deviation of the direction of the incident wave from the exact Bragg conditions: a deviation by the angle φ corresponds to $\alpha = 2\varphi\sin 2\theta$. (In Fig. 1, the distance $LM = \varphi\kappa = \alpha\kappa/2\sin 2\theta$.)

As we see from (2.13) and (2.14), the intensities of the transmitted and diffracted waves are spatially modulated with the period $l = \Lambda/[1 + (\alpha/2\chi_1')]^{1/2}$. If we take account of the absorption, the oscillation in intensity ceases at a depth of the order of $l_1 \approx \mu_1^{-1}[1 + (\alpha/2\chi_1')^2]^{1/2}$, and when $z \gg l_1$, a Borrmann wave field is formed. Extinction modulation ceases at a depth of the order of

$$l_1 = \cos\theta\cdot(\chi_1''\varkappa)^{-1}[1 + (\alpha/2\chi_1')^2]^{1/2} \approx (\mu_1/2)^{-1}[1 + (\alpha/2\chi_1')^2]^{1/2},$$

that corresponds to absorption of the Bloch wave of the first type. Only the Bloch wave of the second type is propagated in the region $z > l_1$ (the Borrmann effect). This wave shows relatively weak absorption, and vanishes at a depth of the order of

$$l_2 = \varkappa^{-1}\cos\theta/\{\chi_0'' - \chi_1''[1 + (\alpha/2\chi_1')^2]^{-1/2}\}.$$

When $|\alpha| \ll |\chi_1'|$, the Borrmann field extends to the maximum depth $l_2 \approx \mu_2^{-1}$. The value of l_2 declines rapidly with increasing deviation from the Bragg angle. When $|\alpha| > |\chi_1'|$,

$$l_2 \approx l_1/\{[1 + (\alpha/2\chi_1')^2]^{1/2} - 1\} \approx (\mu_1/2)^{-1}/\{1 - [1 + (\alpha/2\chi_1')^2]^{-1/2}\}.$$

When the ratio $|\alpha/\chi_1'|$ becomes several times unity (here the deviation of the incident wave from the exact Bragg direction amounts to about 10—15 seconds of angle), l_2 approaches l_1, and the Borrmann effect vanishes completely.

d) Imaging of the surface relief and shape of a crystal. If the exit face of a crystal is not parallel to its entrance face, the extinction modulation of (2.13) and (2.14) gives rise to extinction fringes in the x-ray image of a crystal whose thickness does not exceed l_1. These bands are analogous to the equal-thickness fringes known in optics. In the diffracted-wave image they correspond to specimen thicknesses of half-integral numbers of periods of the extinction modulation $t = l(n + \frac{1}{2})$ $(n = 0, 1, 2, \ldots)$. A very simple example is the image of a wedge-shaped crystal in which the fringes are parallel to the apex of the wedge, and are arranged with a spacing of l/ψ, where ψ is the wedge angle. The systems of interference fringes for the different polarization directions are superimposed. Beating arises here in the image of the wedge, with the period $l' = 2l(1 - C)$. These beats are well marked when $l' < l_1$.

Figure 2 shows an x-ray diffraction photograph of a silicon crystal ($\overline{111}$ reflection; equal-thickness extinction fringes can be seen along the edges of the specimen, and dislocations and macroscopic defects of the crystal are seen in the central part). The contours of the equal-thickness fringes pictorially convey the pyramidal shape of the crystal. By using a photograph

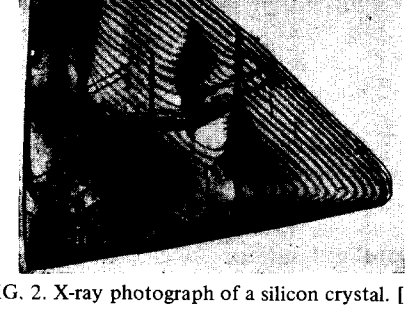

FIG. 2. X-ray photograph of a silicon crystal. [19]

like Fig. 2, one can determine the extinction distance Λ and the value of χ_1' from the spacing between the extinction fringes. The attenuation of the fringes gives the distance l_1 and, correspondingly, the absorption coefficient of the Bloch waves of the first type and the value of χ_1''. As we see from (2.13) and (2.14), the extinction fringes correspond to constant values of the product $t[(\chi_1'/2)^2 + (\alpha/4)^2]^{1/2}$. Hence, equiinclination interference fringes corresponding to contours having α = const. can arise in an equal-thickness plate irradiated by a divergent x-ray beam. Fringes of this type also arise upon bending thin crystal plates, and they permit one to determine the shape of the specimen.

3. WAVE PACKETS IN AN IDEAL CRYSTAL

A spatially inhomogeneous wave field $\mathbf{E}(\mathbf{r})$ can be represented as a superposition of the Bloch waves of (2.3). In general, however, this requires an unlimited choice of Bloch waves. It is more convenient to represent a spatially inhomogeneous field as a superposition of two wave packets that correspond to the transmitted and diffracted waves:

$$\mathbf{E}(\mathbf{r}) \approx \mathbf{E}_0(\mathbf{r})\, e^{i\kappa r} + \mathbf{E}_1(\mathbf{r})\, e^{i(\kappa+\mathbf{K}_1)r}, \tag{3.1}$$

where $\mathbf{E}_0(\mathbf{r})$ and $\mathbf{E}_1(\mathbf{r})$ are smoothly varying functions of the coordinates.

Let us introduce the dimensionless Cartesian coordinates $x = [(\mathbf{K}_1\cdot\mathbf{r})/(\kappa\cdot\mathbf{K}_1)]\kappa^2$ and $z = [((2\kappa + \mathbf{K}_1)\cdot\mathbf{r})/((2\kappa+\mathbf{K}_1)\cdot\kappa)]\kappa^2$ in the scattering plane. Upon substituting (3.1) into (2.1) and neglecting the small longitudinal component of the electric field in the crystal, we get in this coordinate system the following system of equations for each of the two possible polarization directions:

$$\begin{pmatrix} -2i\left(\frac{\partial}{\partial z}+\frac{\partial}{\partial x}\right)-\chi_0 & -\chi_{-1}C \\ -\chi_1 C & -2i\left(\frac{\partial}{\partial z}-\frac{\partial}{\partial x}\right)-\chi_0+\alpha \end{pmatrix}\begin{pmatrix} E_0 \\ E_1 \end{pmatrix} = 0. \tag{3.2}$$

The substitution $E_0 \to E_0 e^{i\chi_0 z/2}$; $E_1 \to E_1 e^{i\chi_0 z/2}$ converts (3.2) to the form

$$\begin{pmatrix} -2i\left(\frac{\partial}{\partial z}+\frac{\partial}{\partial x}\right) & -\chi_{-1}C \\ -\chi_1 C & -2i\left(\frac{\partial}{\partial z}-\frac{\partial}{\partial x}\right)+\alpha \end{pmatrix}\begin{pmatrix} E_0 \\ E_1 \end{pmatrix} = 0, \tag{3.3}$$

For the amplitudes E_0 and E_1, this corresponds to a telegraphic equation with constant coefficients:

$$\hat{D}[E_j] \equiv \left[\frac{\partial^2}{\partial z^2} - \frac{\partial^2}{\partial x^2} + \frac{i\alpha}{2}\left(\frac{\partial}{\partial z}+\frac{\partial}{\partial x}\right) + \frac{\chi^2}{4}\right]E_j = 0, \quad \chi^2 = \chi_{-1}\chi_1 C^2 \quad (j=0,1). \tag{3.4}$$

a) Green's functions. The general solution of Eq. (3.4) can be constructed by means of a Riemann function[20] that differs from zero in the region $|x| \le z$:

$$G(x, z) = -0.5 J_0(0.5\chi(z^2 - x^2)^{1/2})\, e^{-i\alpha(z-x)/4}\, \theta(z)\,[\theta(x+z) - \theta(x-z)]; \tag{3.5}$$

Here $J_0(t)$ is the zero-order Bessel function, and $\theta(t)$ is a step function: $\theta(t) = 0$ when $t < 0$, and $\theta(t) = 1$ when $t > 0$. Let the values of the function $E_j(x, z)$ and its normal derivative $\partial E_j(x, z)/\partial n$ be known on a contour L that intersects the characteristics $z + x$ = count in only one point. For every point (x, z) of the triangular region formed by the contour L and the characteristics drawn from its ends, the values of $E_j(x, z)$ are defined by the expression

$$\begin{aligned} E_j(x, z) = &\int_L dl\,(dx' - dz')\,\frac{i\alpha}{2}\,E_j(x', z')\,G(x-x', z-z') \\ &+ \int_L dl\left[\left(\frac{dz'}{dl}\right)^2 - \left(\frac{dx'}{dl}\right)^2\right]\left[\frac{\partial E_j}{\partial n}(x', z')\,G(x-x', z-z')\right. \\ &\left. - E_j(x', z')\,\frac{\partial G(x-x', z-z')}{\partial n}\right] + 2\int_L dl\,\frac{dx'}{dl}\,\frac{dz'}{dl} \\ &\times\left[\frac{\partial E_j(x', z')}{\partial l}\,G(x-x', z-z') - E_j(x', z')\,\frac{\partial G}{\partial l}(x-x', z-z')\right]. \end{aligned} \tag{3.6}$$

Equation (3.6) stems in an obvious way from Green's theorem if we consider the fact that the Riemann function of (3.5) satisfies the equation

$$\hat{D}[G(x, z)] = -\delta(x)\,\delta(z).$$

If we use (3.2) to eliminate the derivatives $\partial E_j/\partial n$ and $\partial E_j/\partial l$ from Eq. (3.6), we get

$$\begin{aligned} E_0(x, z) = &\int_L (dx' + dz')\,G_{01}(x-x', z-z')\,E_1(x', z') \\ &+ \int_L (x' - dzd')\,G_{00}(x-x', z-z')\,E_0(x', z'), \\ E_1(x, z) = &\int_L (dx' - dz')\,G_{10}(x-x', z-z')\,E_0(x', z') + \\ &+ \int_L (dx' + dz')\,G_{11}(x-x', z-z')\,E_1(x', z'); \end{aligned} \tag{3.7}$$

Here

$$\begin{aligned} G_{01}(x, z) &= -(i\chi_{-1}C/4)\,e^{-i\alpha(z-x)/4}\,J_0(\chi(z^2-x^2)^{1/2}/2)\,\theta(z)\,[\theta(x+z) \\ &\qquad -\theta(x-z)], \\ G_{10}(x, z) &= \\ &= -(i\chi_1 C/4)\,e^{-i\alpha(z-x)/4}J_0(\chi(z^2-x^2)^{1/2}/2)\,\theta(z)\,[\theta(x+z)-\theta(x-z)], \\ G_{00}(x, z) &= -e^{-i\alpha(z-x)/4}\{\delta(z-x) - 0{,}25\chi\,[(z+x)/(z-x)]^{1/2} \\ &\qquad \times J_1(\chi(z^2-x^2)^{1/2}/2)\,\theta(z)\,[\theta(x+z) - \theta(x-z)]\}, \\ G_{11}(x, z) &= -e^{-i\alpha(z-x)/4}\{\delta(z+x) - 0{,}25\chi\,[(z-x)/(z+x)]^{1/2} \\ &\qquad \times J_1(\chi(z^2-x^2)^{1/2}/2)\,\theta(z)\,[\theta(x+z) - \theta(x-z)]\}. \end{aligned} \tag{3.8}$$

The functions of (3.8) are the Green's functions that describe the propagation of a local perturbation of the wave field, and which play the same role in x-ray optics as the function $r^{-1}\exp(i\kappa r)$ does in light optics; according to the Huygens-Fresnel principle, the latter function describes the propagation of a perturbation from an elementary source. The Green's functions of (3.8) differ from zero only in the so-called Borrmann delta $|x| \le z$.

The nature of the propagation of a perturbation within the Borrmann delta depends substantially on the x-ray absorption in the crystal. In weakly absorbing

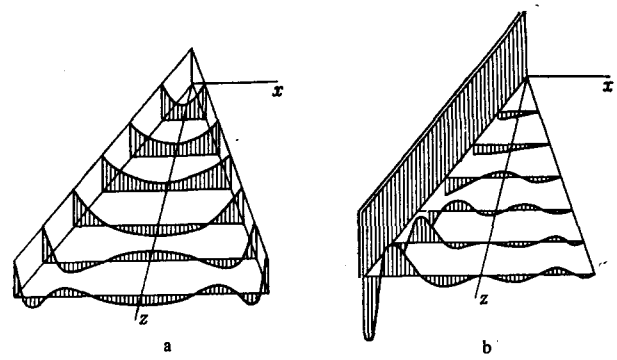

FIG. 3. Diagram of the propagation of a local perturbation.

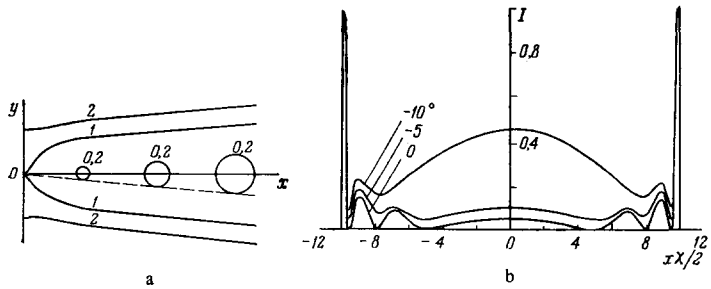

FIG. 4. Effect of absorption on the propagation of a local perturbation.

(thin) crystals having $\mu t < 1$, we can consider the coefficient χ to be real. Then the Green's functions are expressed in terms of the Bessel functions J_0 and J_1 of real argument, which oscillate with ever-declining amplitude as the argument increases. Correspondingly, oscillations arise near the boundaries of the Borrmann delta (near the characteristics), and their number depends on the distance from the perturbation source. We see from (3.8) that the functions G_{00} and G_{11} have δ-type singularities at the characteristics $z = \pm x$, respectively. These singularities can be interpreted as direct geometric images of the source. Figure 3 shows schematically the variation of the Green's functions for a nonabsorbing crystal in exact Bragg orientation ($\alpha = 0$) when a) $i\chi_1(x, z) = i\chi_{-1}G_{10}(x, z)$, and b) $G_{11}(x, z) = G_{00}(-x, z)$.

In absorbing crystals, we must take account of both the real ($\chi' \approx C(\chi'_1\chi'_{-1})^{1/2}$) and the imaginary

$$\chi'' \approx -0{,}5C\,[\chi''_1\,(\chi'_{-1}/\chi'_1)^{1/2} + \chi''_{-1}\,(\chi'_1/\chi'_{-1})^{1/2}]$$

components of the coefficient $\chi = \chi' + i\chi''$. (For the indicated choice of signs $\chi' > 0$ and $\chi'' < 0$.) Since $|\chi''| \ll \chi' \approx |\chi|$, the spatial distribution of the perturbation differs little from the case of a nonabsorbing crystal for small values of $(z^2 - x^2)^{1/2}$ (near the edges of the Borrmann delta). We need only take account of the overall attenuation of the perturbation with depth that follows the law $\exp(-\chi''_0 z/2)$. However, as the argument of the Bessel functions increases, their (absolute) value ceases to oscillate, and it begins to increase exponentially. Consequently, the perturbation is not localized at the edges, but in the central part of the Borrmann delta. To illustrate the behavior of the Green's functions G_{01} and G_{10}, Fig. 4a gives a picture of the modulus of the function $J_0(\rho e^{i\varphi})$ (the dotted line corresponds to $\varphi = \tan^{-1}(y/x) = -5°$). We see from Fig. 4a that the relief of the function $|J_0(x + iy)|$ in the xy plane, where $x + iy = \rho e^{i\varphi}$, is a trough stretching along the x axis. It goes over into steep slopes with increase in the imaginary component y of the argument. The rays $\varphi = \text{const}$. correspond to values $\chi'' = -|\chi| \sin\varphi$. If we assume that $\rho = |\chi|(z^2 - x^2)^{1/2}/2$, we get the intensity distribution of the radiation within the Borrmann delta for a point source, which is schematically shown in Fig. 4b (the intensity distribution of the diffraction image of a narrow slit for $|\chi t| = 20$ as a function of the absorption coefficient as constructed from the relief of Fig. 4a; the value of the parameter φ is indicated on the curves). If we use the asymptotic representation of Bessel functions for large arguments, we can convince ourselves that the transition from oscillations to exponential growth of the Green's functions in the central part of the Borrmann delta occurs at $(z^2 - x^2)^{1/2} \gtrsim -1/\chi''$. This corresponds to attenuation of the Bloch waves of the first type and appearance of a Borrmann wave field. In this region, the perturbations due to the point sources are distributed according to the law $(z^2 - x^2)^{-1/2} \cdot \exp[-\chi''(z^2 - x^2)^{1/2}]$. When $|x| \ll z$, this approaches a Gaussian law having a half-width of the peak of the order of $(z/\chi'')^{1/2}$. The intensity decline with depth for the central part of the Borrmann delta is described by the function $z^{-1}\exp[-(\chi''_0 + \chi'')z]$, and it is determined chiefly by the absorption of the Bloch waves of the second type.

b) Image of a slit and a screen. The Green's functions of (3.8) permit one directly to construct the wave field for an arbitrary distribution of the incident wave on the entrance surface of the crystal. For example, let this surface coincide with the plane $z = 0$. If we assume that $E_0 = E_0(x, y)$ and $E_1 = 0$ for $z = 0$, we obtain from (3.7)

$$\begin{aligned} E_0(x, y, z) &= \int E_0(x', y)\, G_{00}(x - x', z)\, dx', \\ E_1(x, y, z) &= \int E_0(x', y)\, G_{10}(x - x', z)\, dx'. \end{aligned} \tag{3.9}$$

When $E_0(x', y, 0) = \text{const}$., we obtain by using the tabulated integral:

$$\int_{-z}^{z} J_0(\chi(z^2 - x^2)^{1/2}/2)\, e^{i\alpha x/4} dx = 2\sin\{z(\chi^2/4) + (\alpha^2/16)]^{1/2}\}/[(\chi^2/4) + (\alpha^2/16)]^{1/2}.$$

From (3.9), again we get the wave field of (2.13) and (2.14) for an incident plane wave. In the opposite limiting case of an infinitely narrow slit, its image is given directly by the functions G_{00} in the transmitted wave and G_{10} in the diffracted wave. Thus, Figs. 3 and 4 can be treated as being the image of a narrow slit for nonabsorbing and absorbing crystals.

The image of a semiinfinite screen arises from (3.9) with $E_0(x, y) = \mathscr{E}\theta(x)$. The characteristics passing through the edge of the screen dissect the image into three characteristic regions (Fig. 5a), The field is totally absent in the region $x < -z$ (the umbra region I). In the region $x > z$ (the fully illuminated region II), the wave field does not depend on x, and is defined by Eqs. (2.13) and (2.14). An interference image of the screen arises in the transition region $|x| < z$ (the image of the edge of the screen, or region III), which we cannot generally treat as a penumbra region. Figure 5b gives a diagram of the image of a slit (region IV) that is analogous to Fig. 5a. In this case, $E_0(x, y) = \mathscr{E}[\theta(x + a) - \theta(x - a)]$, where a is the half-width of the slit. In regions I–III, the image coincides with the corresponding portion of the image of a screen. In region IV, the interference images of the two screens that form the slit are superimposed. In

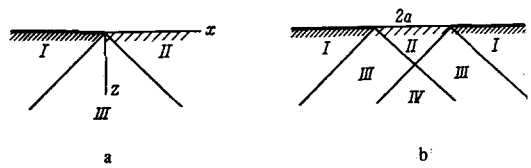

a b

FIG. 5. Diagram of the images of a semi-infinite screen (a) and of a slit (b).

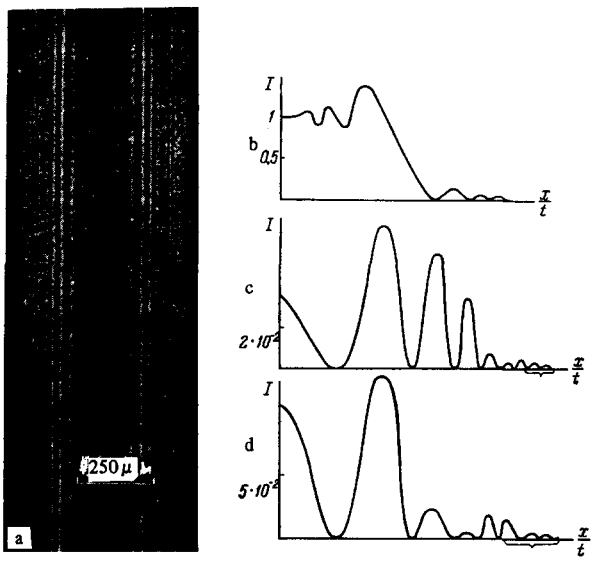

FIG. 6. Diffraction images of a slit and of a semi-infinite screen.

this region, the effect of the slit width on the nature of the image mainly influences the extinction modulations near the boundaries of the region: as compared with the image of an infinitely narrow slit, the extinction fringes that are situated at distances smaller than the slit width vanish. A calculation of the images of a screen and of a finite slit of varying width for non-absorbing and absorbing crystals is given in[21,22] As an illustration, Fig. 6a gives a photograph of a narrow slit[23] [the slit width $2a = 10\ \mu m$, the Si crystal is of thickness $t = 0.42$ mm, (224) reflection; MöKα]. Figures 6b–d give typical examples of calculation of images of a screen (b) and a slit (c, d). (In b, the edge of the screen is at $\alpha = 0$, and $\chi t = 11\pi$:, in c and d, the slit has, respectively, $a/t = 0.625$ and $a/t = 0.125$; we assume that $\alpha = 0$ and $\chi t = 16\pi$; the curly brackets mark the region $|x - t| < a$.)

One can analyze the images of screens and slits qualitatively by analogy with the method of Fresnel zones known in optics. In order to do this, one must distinguish in (3.9) the contribution from the regions corresponding to different signs of the Green's functions. In particular, when $\alpha = 0$, these regions are strips that lie between consecutive zeros of the Bessel functions. For example, let us arrange a zone plate on the surface of a plate of thickness z that consists of a series of opaque screens that cover the intervals between the odd and the following even zeros of the function $J_0(\chi(z_0^2 - x^2)^{1/2}/2)$. Then a brightly illuminated strip will appear on the exit face of the crystal near the line $x = 0$. This band can be used as a line source of x-rays. The intensity of such a diffraction slit increases in proportion to the square root of the thickness of the crystal.

The wave field that arises when a beam of plane waves of different wave vectors is incident on a crystal can be reduced to the above-discussed case of a plane wave: the distribution of the plane waves over their wave vectors κ is equivalent to their distribution over the parameter α. A change of the wave vector by $\delta\kappa$ corresponds to a change in the parameter α by $\delta\alpha = 2\kappa^{-2}\mathbf{K}_1 \cdot \delta\kappa$. This is equivalent to introducing an additional spatial modulation of the wave packet by the coefficient $\exp[-i(\delta\alpha/4)(x - z)]$. Thus, angular divergence of the x-ray beam can be replaced by an equivalent spatial diffuseness of the wave packet.

In the case of an incoherent divergent beam, the waves having different values of α do not interfere with each other, and the integrated intensity of the image is determined by the sum of intensities of the images for waves of all directions. For an infinitely narrow slit, the wave field with full account of the phase does not depend on the parameter α at all. Owing to this fact, determination of the structural parameters from the interference pattern of a narrow slit proves to be more reliable (the relative accuracy of determining the parameter χ is as good as 10^{-3}–10^{-2} [24,25b,e]) than in the case of the equal-thickness fringes mentioned in Sec. d of Chapter 2. For a coherent divergent beam, the amplitudes of the diffracted waves corresponding to different values of α are added, rather than the intensities. Now, the relation of the Green's function of (3.8) to the parameter α reduces to the appearance of the coefficient $\exp[i(\alpha/4)(z - x)]$. Therefore, in convoluting the external field with the Green's functions, one can integrate over the orientations of the incident waves independently of integrating over the surface of the entrance face. The equivalence of the angular and spatial distributions of the waves in the wave packet permits one to vary the choice of representation of the same packet, depending on the concrete problem.

For example, let the amplitude and phase of the plane waves in a broad wave packet be independent of α in the range where this parameter is small. This is the only essential range for the excitation of the field in the crystal (a cylindrical wave can serve as a particular illustration). Introduction of the form factor $\int \exp[i(\alpha/4)(z - x)]d\alpha$ constricts this packet into a narrow ray that is equivalent to a thin slit on the entrance surface of the crystal. Each plane wave of the wave packet excites in the crystal a wave field of the type of (2.12)–(2.14). Superposition of these fields then gives the field described by the Green's functions of (3.8). In fact, if we integrate the relations (2.12)–(2.14) over the parameter α [taking account of the dependence on α of the wave vector κ that enters into Eq. (2.12), which gives $\kappa \cdot \mathbf{r} = \kappa_0 \cdot \mathbf{r} + 0.25(\alpha - \alpha_0)(z - x)$], and use the tabulated integral

$$\int_{-\infty}^{\infty} \sin\{z[(\chi^2/4) + \alpha^2]^{1/2}\}[(\chi^2/4) + \alpha^2]^{-1/2} e^{i\alpha x} = \begin{cases} \pi J_0(\chi(z^2 - x^2)^{1/2}/2), & 0 < |x| < z, \\ 0, & 0 < z < |x|, \end{cases}$$

we get expressions that give the Green's functions G_{00} and G_{10} for $\kappa = \kappa_0$ and $\alpha = \alpha_0$, after transforming to

dimensionless coordinates. Thus, the Green's functions can be constructed not only by the wave-packet method, as was first done in[21] and independently in[26]. They can also be derived by superposition of plane waves (which was treated even in the classical studies on the dynamical theory of scattering) or by direct study of the diffraction of a cylindrical wave emitted by a source that is placed on the surface of the crystal and is equivalent to a narrow slit.

The last-mentioned method is very similar to that of[25a], which is based on treating a field excited in a crystal by a source of diverging spherical waves that is separated from the entrance surface of the specimen by some distance z_0. An intense wave field in the crystal arises only in a small region close to the correct Bragg orientation. In this region, the spherical wave can be replaced by a wave packet having an amplitude proportional to $r^{-1}\exp(i\kappa r - i\mathbf{\kappa}\cdot\mathbf{r})$. Here κ is the wave vector corresponding to exact satisfaction of the Bragg condition, and $\mathbf{r}$ is the radius vector connecting a point on the entrance surface with the source. We can neglect the variation of the coefficient multiplying the exponential, and take account only of the spatial phase modulation of the wave packet. In the plane of incidence $y = 0$ near the point $x = 0$ that corresponds to the exact Bragg condition, the phase difference $\Delta\psi$ varies according to the law

$$\Delta\psi = \varkappa r - \varkappa r = \varkappa\,[(z_0^2\sec^2\theta + 2z_0 x\,\mathrm{tg}\,\theta + x^2)^{1/2} - z_0\sec\theta - x\sin\theta] \approx (x^2/4z_0)\cos^3\theta,$$

or, in dimensionless coordinates,

$$\Delta\psi \approx x^2\sin^2 2\theta/16z_0.$$

Convolution of the amplitude $e^{i\Delta\psi}$ of the wave packet with the Green's functions of (3.8) gives the wave field in the crystal. The nature of this field is determined by the extent of the stationary-phase region where $|\Delta\psi| \ll 1$, as compared with the width of the Borrmann delta. Plane waves of the type of (2.12)–(2.14) arise beneath the stationary-phase region, and they penetrate into the interior of the crystal to a distance of the order of $z_0^{1/2}$ (in dimensionless units). In the opposite limiting case, the wave field at distances greatly exceeding the extent of the stationary-phase region resembles the image of a thin slit, and it is described by functions of the type of G_{00} and G_{10} (this result was obtained in the original study[25a] by resolving the spherical wave into plane waves and approximately summing expressions like (2.12)–(2.14)). The effective slit width proves to be of the order of the extent of the stationary-phase region. This leads to a corresponding blurring of the oscillations of the field at the edges of the Borrmann delta and of the edges themselves. We should note that a number of studies (see, e.g.[25f]) have actually used under the name "spherical-wave approximation" only the limiting case mentioned above, which corresponds to the Green's function approximation. It is not surprising that these studies have often noted the satisfactory agreement of theory and experiment.

c) Images of defects that cause a local perturbation of the wave field. The Green's functions of (3.8) permit one to find the fundamental features of the pattern of images of bulk defects of a crystal whose dimensions in the scattering plane are small in comparison with the extinction distance. Such defects cause local distortions of the wave field (local attenuation of the field for an absorbing inclusion or a local phase shift for pores and precipitates). The further propagation of these perturbations is described by linear combinations of the functions of (3.8). As we see from Fig. 3, the perturbation in the transmitted wave gives a symmetrical intensity distribution, while that in the diffracted wave gives a sharply asymmetric intensity distribution in the diffraction image. Here the local distortion that gives the kinematical ("direct," in Authier's[8a] terminology) image of the defect is propagated along the characteristics $x + z = \text{const}$. In general, the diffracted wave is attenuated at the opposite edge of the Borrmann delta, and this gives a dynamical shadow image of the defect, while the intensity oscillates in the intermediate region in correspondence with the oscillations in the functions G_{10} and G_{11}. At a distance corresponding to the photoelectric-absorption distance l_1, the cited image details vanish, and the perturbation is concentrated in the central part of the Borrmann delta.

For example, let a small, strongly-absorbing inclusion that extends $2l_0 \ll 1/|\chi|$ in the direction of the reflection vector be situated at a distance z_0 from the plane entrance face of the crystal. The waves E_0 and E_1 arriving at the inclusion are practically completely absorbed by it. According to the complementarity principle, the wave-field distortion here can be represented as a field generated at $z = z_0$ by the local perturbation $E_j = -E_j(z_0, x).\,[\theta(x + l_0) - \theta(x - l_0)]$, where x is measured from the center of the inclusion. According to (3.7) and (3.8), the contribution of the inclusion to the diffracted wave for $|\alpha l_0| \ll 1$ and $\chi((z - z_0)l_0)^{1/2} < 1$ is given by the expression

$$\begin{aligned}&\delta E_1(x, z, z_0)\\ &\approx (\chi l_0/2)\exp[-i(\alpha/4)(z - z_0 - x)]\{iE_0^{(0)}(z_0, 0)\,J_0(\chi[(z-z_0)^2-x^2]^{1/2}/2)\\ &\quad - (2/\chi l_0)E_1^{(0)}(z_0, 0)[\theta(x + l_0 + z - z_0) - \theta(x - l_0 + z - z_0)]\\ &\quad + E_1^{(0)}(z_0, 0)[(z - z_0 - x)/(z - z_0 + x)]^{1/2}J_1(\chi[(z - z_0)^2 - x^2]^{1/2}/2)\},\end{aligned} \tag{3.10}$$

and in the transmitted wave by the expression

$$\begin{aligned}&\delta E_0(x, z, z_0)\\ &\approx (\chi l_0/2)\exp[-i(\alpha/4)(z - z_0 - x)]\{iE_1^{(0)}(z_0, 0)\,J_0(\chi[(z-z_0)^2-x^2]^{1/2}/2)\\ &\quad - (2/\chi l_0)E_0^{(0)}(z_0, 0)[\theta(x + l_0 - z + z_0) - \theta(x - l_0 - z + z_0)]\\ &\quad + E_0^{(0)}(z_0, 0)[(z - z_0 + x)/(z - z_0 - x)]^{1/2}J_1(\chi[(z - z_0)^2 - x^2]^{1/2}/2)\}\end{aligned}$$

(we have assumed for simplicity that $\chi_1 = \chi_{-1} = -\chi$, and $C = 1$).

If one uses experimentally a broad slit, and the inclusion occurs in the fully illuminated region (region II in Fig. 5b), then the function $E_j^{(0)}(z_0, 0)$ can be found by solving the ordinary dynamical problem for plane waves (see (2.3) and (2.14)).

The contrast in the image depends on the distance of the inclusion from the entrance face of the crystal. For weakly-absorbing crystals, the contrast depends periodically on the distance z_0 in agreement with the formulas (2.13) and (2.14) for the amplitudes $E_j^{(0)}(z_0)$. In case of anomalous transmission where $z_0 > l_1$, the contrast ceases to depend on z_0, but it continues to depend on the distance of the inclusion from the entrance face. Here the oscillations in the image of the

defect remain as long as the Green's functions continue to oscillate, i.e., until the distance from the entrance face, in turn, exceeds l_1.

If one uses experimentally a narrow slit (sectional topography), the image of a defect depends on its position in the Borrmann delta formed by the slit. In this case we must use as the function $E_j^{(0)}(z_0, 0)$ the functions $\int_{-a}^{a} G_{j0}(-x_0 - x', z_0)dx'$, where x_0 is the coordinate of the center of the slit, and a is the half-width of the slit. Apart from details of extent greater than a and l_0, the contribution of the inclusion to the diffracted wave is given by the formula

$$\delta E_1(x, z, z_0, x_0) \approx -\mathscr{E}(\chi^2 a l_0/4)\exp[-i(\alpha/4)(z + x_0 - x)] \times \{(4i/\chi)\,\delta(z + x - z_0)\,J_0(\chi(z_0^2 - x_0^2)^{1/2}/2) - i[(z-z_0-x)/(z-z_0+x)]^{1/2}\,J_0(\chi[(z-z_0)^2 - x^2]^{1/2}/2)\,J_1(\chi(z_0^2 - x_0^2)^{1/2}/2) + (4i/\chi)\,\delta(z_0 + x_0)\,J_0(\chi[(z - z_0)^2 - x^2]^{1/2}/2) - i[(z_0 - x_0)/(z_0 + x_0)]^{1/2}\,J_0(\chi[(z - z_0)^2 - x^2]^{1/2}/2)\,J_1(\chi(z_0^2 - x_0^2)^{1/2}/2)\}. \quad (3.11)$$

We note that the function $\delta E(x, z, z_0, x_0)$ is invariant except for phase with respect to the substitution $x \rightleftarrows x_0$, $z - z_0 \rightleftarrows z_0$. That is, the contribution of the inclusion to the image does not change when we interchange the center of the entrance slit and the observation point (the reciprocity principle).

If the dimensions of an inclusion or pore are not small in comparison with the extinction distance, then we cannot consider the field to be fixed over the contour of the inclusion. In this case, application of Green's theorem to a doubly-connected region surrounding the inclusion gives by analogy with (3.6) a relation in integral form between the value of the field in the crystal and the field values on the contour of the inclusion. Determining the values of the field on the contour of the inclusion requires that we study the nature of propagation of the wave field within the inclusion. In the case of a cavity (and also for a strongly distorted region like a dislocation nucleus, in which one is allowed to neglect diffraction scattering[27a]), the amplitudes E_0 and E_1 within the "inclusion" are transmitted along the corresponding characteristics. Consequently, the problem of determining the field on the contour of the inclusion is reduced to stepwise solution of the integral equations for regions in which we know the value of one of the amplitudes, E_0 or E_1.

The obtained results can be directly transferred to the case of defects whose axis intersects the scattering plane in a single point. The image of the defect on the exit face will fill a triangular region having its vertex P at the point of emergence of the defect at the surface of the crystal. Its lateral sides PQ and PR will be formed by the characteristics passing through the axis of the defect. In the symmetrical Laue case, the slopes of the rays PQ and PR are, respectively, $(\cos^2\psi - \sin^2\varphi)^{1/2}/(\sin\psi \pm \sin\varphi\tan\theta)$. Here ψ and φ are the angles that the axis of the defect makes with the reflecting plane and with the exit face of the crystal. The angle QPR is a maximum when $\psi = 0$.

If we substitute the equation of the axis of the defect, $(x_0 - xp)\csc\psi = (y_0 - yp)/(\cos^2\psi - \sin^2\varphi)^{1/2} = (z_0 - zp)\csc\varphi$, into Eq. (3.10) or (3.11), we can find the image of the defect on the exit face $z = zp$ of the crystal. In particular, when $z_0 < l_1$, (3.10) implies that an overall periodic variation in contrast in the image should be observed, which is related to the extinction periodicity of the amplitudes $E_j^{(0)}$. Owing to the factor

$$\{|z_P - z_0 - (x - x_0)\operatorname{ctg}\theta|/[z_P - z_0 + (x - x_0)\operatorname{ctg}\theta]\}^{1/2}$$

the most intense image in the diffracted wave arises in a region adjoining the kinematical image PQ of the defect. The function J_1 proves to have the decisive influence on the nature of the contrast. Superposition of the oscillations of $E_0^{(0)}$ on the oscillations of J_1 leads to a discontinuous extinction striation of the image: fringes of hyperbolic shape corresponding to the maxima and minima of J_1 are modulated with the period

$$\Delta y = 2l\operatorname{cosec}\varphi(\cos^2\psi - \sin^2\varphi)^{1/2}. \quad (3.12)$$

In the case $z_0 > l_1$, which corresponds to observing the defect by the Borrmann method, extinction striation also arises in the region $zp - z_0 < l_1$, and it involves interference between $E_j^{(0)}$ and $E_j^{(0)}(zp)$. The interference fringes modulated with the period of (3.12) again form hyperbola-shaped contours. As in the case $z_0 < l_1$, the brightest fringes arise near the kinematical image of the defect: the general pattern of the image in this image resembles the above-discussed case in which $z_0 < l_1$. When $zp - z_0 > l_1$, the extinction fringes disappear, and the pattern of the image gradually acquires a simple form, and is composed of the shadow of the defect bordered by fringes of increased intensity (black-white-black contrast;[10b] see also Sec. a of Chap. 5). When the defect is situated at a depth $zp - z_0 > l_2$, the image finally blurs and vanishes. Figure 7 illustrates schematically the discussed features of the image of a linear defect. The axis of the defect intersects the exit face at the point P, and the line PQ corresponds to the kinematical

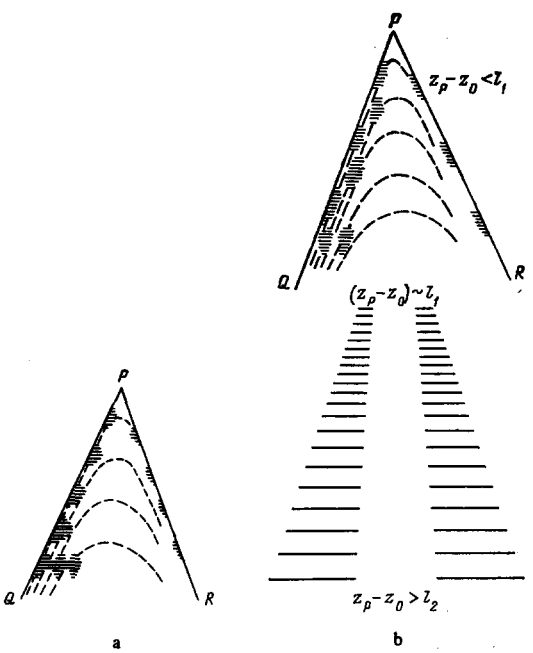

FIG. 7. A diagram of the image of a rectilinear defect constructed by using the Green's functions.

FIG. 8. Photograph of an inclined 72° dislocation in silicon. [28]

image. The regions of increased image intensity are indicated by cross-hatching. The positions of the maxima of the functions $|J_1(0.5\chi((z^2 - x^2)^{1/2})|$ are shown by the dotted lines (a is for a thin crystal ($zp < l_1$); b is for a thick crystal ($Zp \gg l_1$); the image for the region $z_p - z_0 < l_1$ resembles case a). Figure 8 shows a typical photograph of an inclined dislocation with the characteristic extinction striation of the image in the region adjoining the direct image of the defect (Si crystal in the (220) reflection, MoKα).

The presented treatment has dealt with a case in which the defect causes a local perturbation of one given sign. If the perturbation at the wave front consists of two neighboring peaks of opposite signs, the overall picture of the image is given in the first approximation by the derivatives of the Green's functions of (3.8) with respect to x. An inclined edge dislocation or one parallel to the surface of the crystal gives rise to an image of the first or second type, depending on whether its Burgers vector is parallel or perpendicular to the reflection vector.

4. THE WAVE FIELD IN AN INHOMOGENEOUS CRYSTAL

In a real crystal, owing to lattice distortions, the polarizability $\chi(\mathbf{r})$ ceases to be a strictly periodic function of the coordinates, and it depends on the displacement field $\mathbf{u}(\mathbf{r})$. For a smooth displacement field, the distortions $\partial u_i/\partial x_k$ are small, and we can assume that the inner electron clouds that are responsible for x-ray scattering remain undistorted, and are only shifted along with the atoms. That is, the variation in the polarizability reduces to a change in the argument of the function $\chi(\mathbf{r})$ by the amount of the displacement vector $\mathbf{u}(\mathbf{r})$. In this case, χ_h on the right-hand side of (2.2) becomes $\chi_h \exp[-i\mathbf{K}_h \cdot \mathbf{u}(\mathbf{r})]$, while Eq. (3.2) takes on the form

$$\begin{pmatrix} 2i\left(\frac{\partial}{\partial z}+\frac{\partial}{\partial x}\right)+\chi_0 & \chi_{-1}Ce^{-i\mathbf{K}_1\mathbf{u}(\mathbf{r})} \\ \chi_1 Ce^{-i\mathbf{K}_1\mathbf{u}(\mathbf{r})} & 2i\left(\frac{\partial}{\partial z}-\frac{\partial}{\partial x}\right)+\chi_0-\alpha \end{pmatrix}\begin{pmatrix} E_0 \\ E_1 \end{pmatrix}=0. \qquad (4.1)$$

The substitution $E_0 \to E_0 \exp(i\chi_0 z/2)$, $E_1 \to E_1 \exp[i(\chi_0 z/2) - i\mathbf{K}_1 \cdot \mathbf{u}(\mathbf{r})]$ puts (4.1) into the canonical form

$$\begin{pmatrix} 2i\left(\frac{\partial}{\partial z}+\frac{\partial}{\partial x}\right) & \chi_{-1}C \\ \chi_1 C & 2i\left(\frac{\partial}{\partial z}-\frac{\partial}{\partial x}\right)-\alpha(\mathbf{r}) \end{pmatrix}\begin{pmatrix} E_0 \\ E_1 \end{pmatrix}=0, \qquad (4.2)$$

as was first pointed out by Takagi.[29a] It differs from (3.3) in the dependence of the parameter α on the coordinates:

$$\alpha(\mathbf{r}) = \alpha - 2\left(\frac{\partial}{\partial z}-\frac{\partial}{\partial x}\right)\mathbf{K}_1\mathbf{u}(\mathbf{r}). \qquad (4.3)$$

The substitution used in deriving (4.2) has no effect on the boundary conditions for the amplitudes E_0 and E_1, which maintain the same form as for an ideal crystal.

According to (4.3), the effect of the distortion field on the wave field is determined by the displacements of the reflecting planes alone. Hence, in particular, edge dislocations parallel to the reflection vector and screw dislocations perpendicular to this vector will give no x-ray image.

Equation (4.2) is equivalent to the following telegraphic equations with variable coefficients for the amplitudes E_0 and E_1:

$$\hat{D}_0[E_0] \equiv \left[\frac{\partial^2}{\partial z^2}-\frac{\partial^2}{\partial x^2}+\frac{i\alpha(\mathbf{r})}{2}\left(\frac{\partial}{\partial z}+\frac{\partial}{\partial x}\right)+\frac{\chi^2}{4}\right]E_0=0,$$

$$\hat{D}_1[E_1] \equiv \left[\frac{\partial^2}{\partial z^2}-\frac{\partial^2}{\partial x^2}+\frac{i\alpha(\mathbf{r})}{2}\left(\frac{\partial}{\partial z}+\frac{\partial}{\partial x}\right)+\frac{i}{2}\left(\frac{\partial\alpha(\mathbf{r})}{\partial z}+\frac{\partial\alpha(\mathbf{r})}{\partial x}\right)+\frac{\chi^2}{4}\right]E_1=0. \qquad (4.4)$$

As in the case of constant coefficients, the general solution of these equations[20] has a form resembling (3.6). However, here the Riemann functions $G_0(z, x, z', x')$ and $G_1(z, x, z', x')$ are, respectively, the Green's functions for the conjugate equations

$$\hat{D}_0^*[G_0] \equiv \left[\frac{\partial^2}{\partial z'^2}-\frac{\partial^2}{\partial x'^2}-\frac{i\alpha(\mathbf{r}')}{2}\left(\frac{\partial}{\partial z'}+\frac{\partial}{\partial x'}\right)-\frac{i}{2}\left(\frac{\partial\alpha(\mathbf{r}')}{\partial z'}+\frac{\partial\alpha(\mathbf{r}')}{\partial x'}\right)+\frac{\chi^2}{4}\right]G_0=-\delta(x-x')\,\delta(z-z'),$$

$$\hat{D}_1^*[G_1] \equiv \left[\frac{\partial^2}{\partial z'^2}-\frac{\partial^2}{\partial x'^2}-\frac{i\alpha(\mathbf{r}')}{2}\left(\frac{\partial}{\partial z'}+\frac{\partial}{\partial x'}\right)+\frac{\chi^2}{4}\right]G_1=-\delta(x-x')\,\delta(z-z').$$

As in the case of (3.8), the Green's functions differ from zero only in a triangular region (the Borrmann delta) bounded by the characteristics $z + x = \text{const}$.

The representation of the wave field in an inhomogeneous crystal in terms of Riemann functions has been discussed in detail in[29b]. However, this representation is only a formal way of writing down the solution, since the Riemann function in an inhomogeneous crystal no longer shows translational symmetry, and it depends in a complicated way on all four arguments x, x', z, and z'.

This explains why it has not been possible in any of the studied practical cases to establish the explicit form of the Riemann functions.

A number of examples of x-ray images of crystal defects that give rise to known distortion fields have been calculated numerically with a computer from Takagi's equations. Taupin[30] and Authier and his associates[28,31] have calculated various cases of images of screw and edge dislocations lying parallel and inclined to the surface of the crystal. In[32] they calculated the image of an edge dislocation perpendicular to the surface of the specimen. Figure 9 shows characteristic examples of the calculated image for edge dislocations having different orientations (a is an edge dislocation parallel to the surface of the crystal;[30] b is a mixed dislocation inclined to the surface of the crystal;[28] and c is an edge dislocation perpendicular to the surface of the crystal[32]). Contour lines for the intensity distribution of the image in the diffracted wave are shown in planes respectively parallel (a) and perpendicular (b and c) to the scattering plane. The coordinate net is plotted in Fig. 9a in units of $2\Lambda/\pi$. If we compare Figs. 9a and b with Fig. 7, we can convince ourselves that the fundamental details of the image often depend weakly on the type of linear defect being observed, and are fixed mainly by the Green's functions. A common feature of Figs. 9a, b, and c is the deflection of the diffracted radiation away from the strongly distorted region to distances that greatly ex-

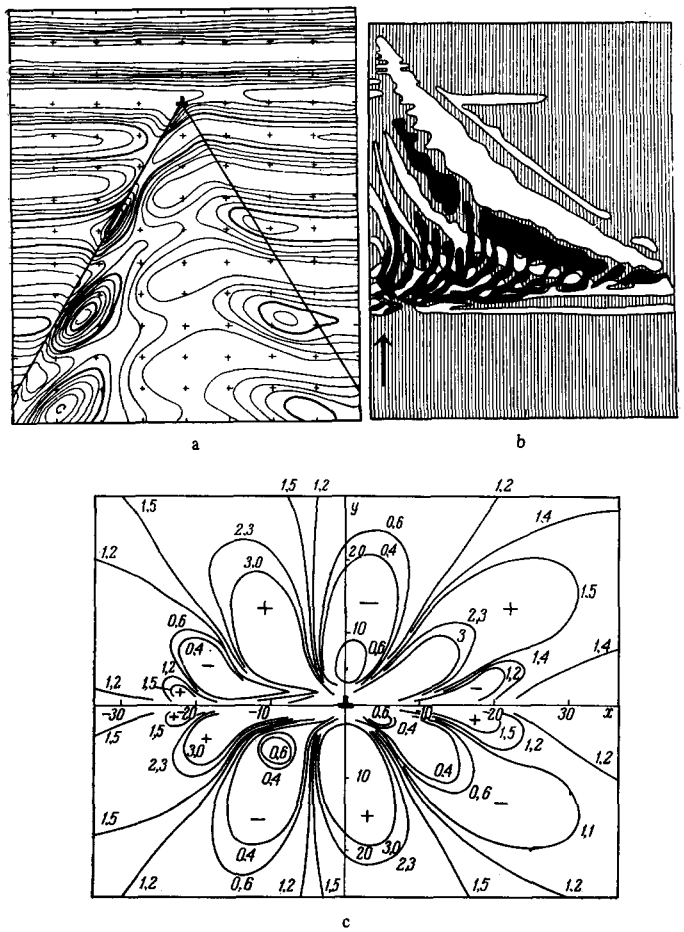

FIG. 9. Examples of calculated dislocation images.

FIG. 10. Photograph of an edge dislocation perpendicular to the surface of a silicon crystal. [33]

ceed the dimensions of this region and that are determined by the cross-section of the Borrmann delta. This effect is well marked on photographs of edge dislocations perpendicular to the surface of the crystal (Fig. 10).

By analogy with the atlasses of electron-microscopic images like[16,34], one could seemingly compile by numerical calculation atlases of x-ray diffraction images of characteristic defects for various orientation cases and various values of the dynamical-scattering parameters. Owing to the variety of different cases, it is hard to say how effective this approach will be in comparison with semiqualitative analytical study of images by approximate solution of Eq. (4.2).

We can point out some special cases that simplify analytical solution of Takagi's equations. In the symmetrical case of Laue diffraction with $\mathbf{K}_1 \cdot \mathbf{u}(\mathbf{r}) = f(z)$ and uniform illumination of the crystal, the wave field ceases to depend on the variable x, and the system (4.2) reduces to a system of ordinary differential equations:

$$\begin{pmatrix} 2i\frac{\partial}{\partial z} & \chi_{-1}C \\ \chi_1 C & 2i\frac{\partial}{\partial z} - \alpha(z) \end{pmatrix} \begin{pmatrix} E_0 \\ E_1 \end{pmatrix} = 0,$$

These coincide with the equations of the columnar approximation in the theory of the electron-microscope image.[16] In order to analyze the image in this case, one can use the results of studying electron-microscope images of lattice defects with the appropriate recalculation of the coefficients of the problem. In particular, one can use these results to analyze the images of dislocations parallel to the reflection vector (a special defect position according to Elistratov[8] and Shul'pina[35]).

In particular, study of dislocations parallel to the reflection vector permits one to apply a rule for determining the sign of the dislocation that was developed in diffraction electron microscopy.[16] It is based on the difference between the images for the reflections (hk$l$) and ($\overline{\text{hk}l}$). These reflections differ in the sign of the vector $\mathbf{K}_1$. According to (4.3), this corresponds to changing the sign of the variable part of the parameter $\alpha(\mathbf{r})$, or to changing the sign of the dislocation while the photograph is being taken with the same reflection. Consequently, if we compare the contrast in the x-ray image in the (hk$l$) and ($\overline{\text{hk}l}$) reflections on the two sides of the dislocation, which arises in this case from regions having distortions of opposite signs, we can determine the sign of the Burgers vector of the dislocation.[36] In sectional topography, the images of dislocations parallel to the reflection vector also can be derived by analogy with calculation of an electron-microscope image. If we expand the wave field at the surface of the crystal in a Fourier integral, we can interpret each harmonic $E(\alpha)\exp(-i\alpha x/4)$ as resulting from incidence of a plane wave having a changed wave vector and the appropriate parameter α (cf. Sec. b of Chap. 3). Just as in electron microscopy, such a wave will give rise to a plane wave field (independent of the coordinate x) and a certain reflection $E_j(y, \alpha)$ of the dislocation on the exit face of the crystal. The latter can be treated as a Fourier component of the image in sectional topography. In fact, sectional topography permits one to carry out interferometry of the distortion field. Fourier synthesis permits one to reconstruct the sought image

$$E_j(x, y) = \int_{-\infty}^{\infty} e^{-i\alpha x/4} E_j(y, \alpha)\, d\alpha, \qquad (4.5)$$

and conversely, Fourier analysis of the sectional image $E_j(x, y)$ gives the image of a defect in a special position in the case of illumination by broad parallel beams having different wave vectors.

Another special case is a distortion field that does not vary along the direction of the diffracted beam, i.e., the case in which $\mathbf{K}_1 \cdot \mathbf{u}(\mathbf{r}) = f(z + x)$. According to (4.3), α then proves to be constant and the distortion field does not affect the Bragg condition, nor does it affect the wave field in the transmitted or diffracted wave. Thus the image of the defect completely vanishes.

Finally, in the case $\mathbf{K}_1 \cdot \mathbf{u}(\mathbf{r}) = f(z - z)$, the substitution $E_j \to E_j \exp(i\mathbf{K}_1 \cdot \mathbf{u}(\mathbf{r}))$ converts the system (4.2) to the form (3.3), and the solution can be found in explicit form under arbitrary boundary conditions. If $E_0(x, y, 0) = \mathcal{E}(x, y)$, then $E_1(x, y, z)$

$= i(\chi_{-1}C/2)\exp[i(\chi_0/2)z - i(\alpha/4)z + i\mathbf{K}_1\cdot\mathbf{u}(z-x)]$
$\times \int_{-z+x}^{z+x} J_0(\chi[z^2-(x-x')^2]^{1/2}/2)\exp[i(\alpha_0/4)(x-x') - i\mathbf{K}_1\cdot\mathbf{u}(-x')]dx'$. In particular, dislocations lying along the direction of the diffracted wave will give no contrast, while (4.5) gives an exact analytic expression for the images of dislocations lying along the direction of the incident wave. Figure 11 illustrates schematically the discussed three cases of special locations of defects ($\mathbf{K}_1\cdot\mathbf{u}(\mathbf{r}) = f(z)$ (diagram a), or $= f(z+x)$ (diagram b), or $= f(z-x)$ (diagram c)).

For very smooth distortion fields, the function $\alpha(\mathbf{r})$ depends weakly on the coordinates. If we assume that $\alpha(\mathbf{r}) = \alpha_0 + \alpha_1(\mathbf{r})$, where $|\alpha_1(\mathbf{r})| \ll |\alpha_0|$, we can transfer the terms involving α_1 in (4.4) to the right-hand side, and treat them as a perturbation. According to[20], the solution of the telegraphic equation (3.4) having the right-hand side

$$\hat{D}[E_j] = -F_j(x, z)$$

is expressed in terms of the Riemann function of (3.5) as follows:

$$\begin{aligned} E_j(x,z) = &\int_L (dx'-dz')\frac{i\alpha_0}{2}E_j(x',z')G(x-x',z-z') \\ &+\int_L dl\left[\left(\frac{dz'}{dl}\right)^2-\left(\frac{dx'}{dl}\right)^2\right]\left[\frac{\partial E_j(x',z')}{\partial n}G(x-x',z-z')\right. \\ &\left.-E_j(x',z')\frac{\partial G(x-x',z-z')}{\partial n}\right]+2\int_L dl\frac{dx'}{dl}\frac{dz'}{dl} \qquad (4.6) \\ &\times\left[\frac{\partial E_j(x',z')}{\partial l}G(x-x',z-z')-F_j(x',z')\frac{dG(x-x',z-z')}{\partial l}\right] \\ &+\int\int dx'\,dz'G(x-x',z-z')F_j(x',z'). \end{aligned}$$

Here the term that is new with respect to (3.6) is an integral of the Riemann function over the Green's function region, i.e., over a triangle formed by the contour L and the characteristics passing through the observation point (x, z). In our case the Riemann function is determined by Eq. (3.5), with α replaced by α_0, and the right-hand side is given by the expression:

$$F_0(x,z) = \frac{i\alpha_1(\mathbf{r})}{2}\left(\frac{\partial}{\partial z}+\frac{\partial}{\partial x}\right)E_0, \quad F_1(x,z) = \frac{i}{2}\left(\frac{\partial}{\partial z}+\frac{\partial}{\partial x}\right)[\alpha_1(\mathbf{r})E_1],$$

Thus Eq. (4.6) gives an integral equation for the sought function $E_j(x, z)$. In the first approximation (see[21]), we replace in $F_j(x, z)$ the function $E_j(x, z)$ by its unperturbed value $E_j^{(0)}(x, z)$, which corresponds to the solution of (4.2) for $\alpha = \text{const}$. (see (2.13) and (2.14)). Then we get the approximate solution $E_j^{(1)}$, which corresponds to the well-known Born approximation in scattering theory. If we replace E_j by the function $E_j^{(1)}$ in F_j, we get a second approximation, etc. A second variant of constructing an approximate solution of Takagi's equations by using (4.6) has been pointed out in.[26] They propose that one should use the Kato-Kambe solution[34] as the zero-order approximation for the function E_j (see Chap. 5 below).

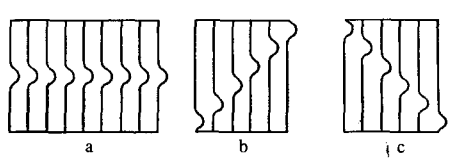

FIG. 11. Special positions of defects that simplify image calculation.

In the case of sharply localized distortion fields, one can multiply the Green's functions of (3.8) by the amplitude of the wave field at the site of the defect, owing to the sign of the double integral in (4.6). If we neglect the self-action and interaction of perturbations arising from defects, and set the amplitude of the field at the site of a defect to be equal to its value in the absence of defects, we again arrive at the approximation treated in Sec. c of Chapter 3.

Finally, if the localized distortion field proves to be so strong that $|\alpha| \gg |\chi|$ near the defect, then we can neglect the quantity χ_{-1} in Eq. (4.1) in comparison with α. Then the inverse effect of the wave E_1 on the wave E_0 will vanish, and the image in the diffracted wave will be determined by kinematical scattering of the transmitted wave. Consequently, the phase of the wave E_1 will be increased by $\mathbf{K}_1\cdot\delta\mathbf{u}$, where $\delta\mathbf{u}$ is the discontinuity in the displacement field arising from the local distortion. [In Eq. (4.1), passage through a region of local perturbation does not change the two components of the wave field.] The initial form of the local distortions of the wave field due to small defects is reduced in this approximation to the perturbation $E_1^{(0)}[\exp(i\mathbf{K}_1\cdot\delta\mathbf{u}) - 1]$ in the diffracted wave, with no perturbation in the transmitted wave. Correspondingly, the image of the perturbation is determined by the Green's functions G_{01} in the transmitted wave, and G_{11} in the diffracted wave.

A characteristic example is the problem of the image of a stacking defect.[9b,25] In this case the variation of the displacement field is exactly reduced to a jump in the displacement field $\delta\mathbf{u}$ at the stacking defect; $\alpha(\mathbf{r})$ is described correspondingly by a boundary δ-function due to the jump in the phase of E_1 by $\mathbf{K}_1\cdot\delta\mathbf{u}$. The image is now given not approximately, but exactly by the Green's functions G_{01} and G_{11}. If the stacking defect intersects the Borrmann delta, superposition of the contributions of each region of this defect in the x-ray image leads to appearance of extinction fringes in the image that resemble equal-thickness fringes.

It is essential to emphasize the fundamental distinction in the nature of the images of regions having strongly localized distortions and of those having weak and smoothly-varying distortions. In the former case, diffracted radiation is deflected away from the distorted region. Many details of the image depend weakly on the nature of the source of perturbation. In particular, the size of the image in the direction of the reflection vector depends on the depth at which the defect is located and the diffraction angle, rather than on the size of the defect. In the latter case, the x-ray contrast directly reflects the deformation field in the given region. The equal-intensity lines and interference fringes directly give the distribution of distortions. If in addition the parameter $\alpha(\mathbf{r})$ varies weakly through the thickness of the specimen, then according to Sec. b of Chap. 3, the interference fringes correspond to lines of constant $|\Delta\mathbf{k}|$, and they can be interpreted as equal-inclination or equal-deformation fringes.[37]

5. GEOMETRICAL X-RAY OPTICS

The mathematical difficulties that arise in constructing the x-ray field in inhomogeneous crystals are ana-

logous to the well-known difficulties of constructing the electromagnetic field when light and radio waves pass through inhomogeneous media. The ray approximation is widely used in optics for media having smoothly varying characteristics (the dimensions L of the inhomogeneities must greatly exceed the wavelength λ). The concept of rays and their trajectories can be introduced even in the case of an x-ray field. However, the criterion for applicability of geometrical optics will no longer be $L \gg \lambda$ here (a condition that always holds), but the more rigid condition $L \gg \Lambda$, where Λ is the extinction distance.

Proceeding by analogy with geometrical optics, we separate out in the amplitudes E_0 and E_1 the rapidly varying phase factors

$$\hat{E} \equiv \begin{pmatrix} E_0 \\ E_1 \end{pmatrix} = e^{iS^{(I)}(x,\,z)}\,\hat{E}^{(I)}(x,\,z) + e^{iS^{(II)}(x,\,z)}\,\hat{E}^{(II)}(x,\,z). \tag{5.1}$$

In contrast to ordinary optics, we have introduced directly two phases (two eikonals), $S^{(I)}$ and $S^{(II)}$, which correspond to the different branches of the dispersion surface. If we substitute (5.1) into Takagi's equation (4.2), we get an equation for determining the amplitudes $\hat{E}^{(I)}$ and $\hat{E}^{(II)}$:

$$(D_S + D)\,\hat{E} = 0, \tag{5.2}$$

where

$$D_S = \begin{pmatrix} -\left(\frac{\partial S}{\partial x} + \frac{\partial S}{\partial z}\right) & \frac{1}{2}\chi_{-1}C \\ \frac{1}{2}\chi_1 C & \left(\frac{\partial S}{\partial x} - \frac{\partial S}{\partial z}\right) - \frac{\alpha(\mathbf{r})}{2} \end{pmatrix}, \tag{5.3}$$

$$D = \begin{pmatrix} i\left(\frac{\partial}{\partial z} + \frac{\partial}{\partial x}\right) & 0 \\ 0 & i\left(\frac{\partial}{\partial z} - \frac{\partial}{\partial x}\right) \end{pmatrix}. \tag{5.4}$$

In order that a non-trivial zero-order approximation should exist that satisfies the equation $D_S\hat{E} = 0$, the determinant of the matrix D_S must vanish. In expanded form, this condition gives an equation for the eikonals $S^{(I)}$ and $S^{(II)}$ in first-order partial derivatives:

$$\{H - [\alpha(\mathbf{r})/4]\}^2 - \{P - [\alpha(\mathbf{r})/4]\}^2 = \chi^2/4; \tag{5.5}$$

Here we have introduced the symbols $H = -\partial S/\partial z$ and $P = \partial S/\partial x$, which permit us to treat the derived equation by analogy with the classical equations for the action, the energy, and the generalized momentum. In contrast to ordinary optics, Eq. (5.5) corresponds to the Hamilton-Jacobi equation for particles having a non-zero rest mass. The trajectories of the rays orthogonal to the surface of the wave fronts S = const., are analogous, for example, to the trajectories of charged particles of mass $\chi/2$ in one-dimensional motion along the x axis in some electric field. We note that Eq. (5.5) contains the complex coefficient χ. Hence, strictly speaking, it is a system of two equations for the real and imaginary parts of the function $S = S' + iS''$. However, the smallness of the imaginary part of χ makes the imaginary part S'' of the eikonal small in comparison with its real part S'. Consequently the equations of the trajectories of the rays for the eikonals S' and S'' coincide. Thus, taking account of the complex nature of the polarizability is reduced to taking account of the attenuation of the amplitude along the trajectory of the rays.

If we assume for simplicity that the coefficient χ in Eq. (5.5) is real, we can interpret this equation as being the equation of the dispersion surface for the

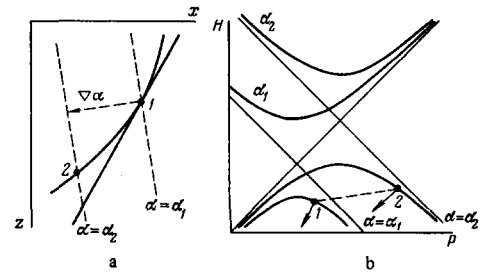

FIG. 12. Course of the weakly absorbed ray in coordinate space (a) and phase space (b).

correction to the wave vector of the Bloch waves. At different sites in the crystal, this surface keeps a constant orientation, but occupies different positions, according to the local value of the parameter $\alpha(\mathbf{r})$: the center of the hyperbolas is shifted along the straight line P = H, being situated at the point having coordinates $(\alpha/4, \alpha/4)$. This is illustrated by Fig. 12b and Fig. 15 to be discussed below. Each value of P on the dispersion surface corresponds to two values of H:

$$H = (\alpha/4) \pm \{(\chi^2/4) + [P - (\alpha/4)]^2\}. \tag{5.6}$$

The upper sign corresponds to the upper branches of the dispersion surface in Fig. 12b and Fig. 15. If we keep the numbering of the branches of the dispersion surface adopted in Chap. 2, we should consider the upper branch to be first, and assign the eikonal $S^{(I)}$ to it. When we take account of the imaginary part $\chi'' < 0$ in the parameter χ, the first branch corresponds to the strongly absorbed Bloch wave, and the second (lower) branch to the weakly absorbed one.

a) Ray trajectories. The ray-trajectory equations arising from (5.5) can be written in a form analogous to the classical Hamilton-Jacobi equations of motion:

$$\frac{dx}{dz} = \frac{\partial H}{\partial P}, \tag{5.7}$$

$$\frac{dP}{dz} = -\frac{\partial H}{\partial x}. \tag{5.8}$$

As is usual, (5.7) and (5.8) imply a law of variation of the energy along the trajectory:

$$\frac{dH}{dz} = \frac{\partial H}{\partial z} + \frac{\partial H}{\partial P}\frac{dP}{dz} + \frac{\partial H}{\partial x}\frac{dx}{dz} = \frac{\partial H}{\partial z}. \tag{5.9}$$

The relations (5.7)–(5.9) establish a simple connection between the ray trajectory in the x, z coordinate space and the wave-vector trajectory in the P, H phase space. If we arrange the coordinate axes as shown in Fig. 12 (with the P axis parallel to the x axis and the H axis antiparallel to the z axis), then the ray trajectory in coordinate space proves to be parallel to the normal to the dispersion surface of (5.5), while the wave-vector trajectory in phase space is antiparallel to the gradient of H, and hence to the gradient of $\alpha(\mathbf{r})$. Shifting the ray from the level line $\alpha = \alpha_1$ to the line $\alpha = \alpha_2$ corresponds to shifting the wave vector from the dispersion surface $\alpha = \alpha_1$ to the surface $\alpha = \alpha_2$. As an example, Fig. 12a shows a region of the trajectory of the weakly absorbed ray, which is traversing this region as $\alpha(\mathbf{r})$ increases. As we see from Fig. 12b, the wave vector increases in its component parallel to the reflection vector.

Using the above-cited analogy of an x-ray trajectory

to that of a charged particle, we can write the equation of the trajectory in a form resembling the equation of motion of a relativistic electron.[38] Equations (5.6) and (5.7) imply a relation of the "velocity" dx/dz to the ordinary momentum p = P − (α/4):

$$p = \pm (\chi/2)\,(dx/dz)/[1 - (dx/dz)^2]^{1/2} \qquad (5.10)$$

(the slopes of the characteristics in our case are ±1, which corresponds to a unit "velocity of light"). When rewritten in terms of the ordinary momentum, Eq. (5.8) gives the trajectory in the form

$$dp/dz = \mathscr{E}(x, z), \qquad (5.11)$$

Here the force $\mathscr{E}(x, z)$, which is equivalent to the external electric field in the case of motion of a particle of unit charge, is determined by

$$\mathscr{E}(x, z) = -\frac{1}{4}\left(\frac{\partial}{\partial z} + \frac{\partial}{\partial x}\right)\alpha(x, z). \qquad (5.12)$$

Upon taking account of (4.3), we can derive from (5.10) −(5.12) the trajectory equation in the form[24b]

$$\pm\frac{\chi}{2}\frac{d}{dz}\left(\frac{dx/dz}{[1-(dx/dz)^2]^{1/2}}\right) = \frac{1}{2}\left(\frac{\partial^2}{\partial z^2} - \frac{\partial^2}{\partial x^2}\right)\mathbf{K}_1\mathbf{u}(\mathbf{r}) \qquad (5.13)$$

(the upper sign corresponds to the upper branch of the dispersion surface, i.e., to the strongly absorbed rays). When $\mathscr{E} > 0$, i.e., when α(r) declines along the direction of the transmitted wave, the weakly absorbed rays are deflected in the direction of the reflection vector, while the strongly absorbed rays are deflected in the opposite direction. When α = α(x), the regions having negative curvature of the function α(x) act on the weakly absorbed rays like converging lenses, but like diverging lenses on the strongly absorbed rays (such lenses can be realized by regulating the dislocation structure of the specimen). The regions having a positive curvature of α(x) exert the opposite effect on the course of the rays. Hence, absorbing crystals under Borrmann-effect conditions show positive contast in regions of the first type, but negative contrast in regions of the second type, as compared with the overall background of the image. This sign rule can be used to determine the signs of distortion fields, and correspondingly, to determine the type of inclusions, the sign of the Burgers vector of dislocations, etc.

If the component u_x of the displacement field in the direction of the reflection vector is a quadratic function of the coordinates, the force $\mathscr{E}$ does not depend on the coordinates. This is equivalent to the well-known case of motion of a charged particle in a d.c. electric field.[38] For example, let a cubic crystal undergo thermal distortion caused by a uniform temperature gradient along the x axis. Then the reflecting planes acquire a spherical shape, and

$$u_x = (1/2R)\,(z^2 + y^2 - x^2), \qquad (5.14)$$

Here R is the radius of curvature of the reflecting planes. According to (5.13) for the field of (5.14), the force $\mathscr{E} = -K_1R^{-1}/2\kappa^2 = \text{const}$. Another example is circular bending of the specimen about the y axis, in which the reflecting planes acquire a cylindrical shape, and $u_x = (\frac{1}{2}R)\,(z^2 + Ax^2)$, where the coefficient A depends on the orientation of the neutral plane and the elastic constants of the crystal. In this case, $\mathscr{E} = -K_1R^{-1}/2\kappa^2(\cos^2\theta - A\sin^2\theta)$.

We see from (5.11) that when $\mathscr{E}$ = const., the momentum p increases linearly with depth in the crystal:

$$p = p_0 + \mathscr{E}z. \qquad (5.15)$$

Equation (5.7) gives the following equation for the slope of the ray:

$$dx/dz = \pm p/[p^2 + (\chi^2/4)]^{1/2},$$

Integration of the latter with account taken of (5.15) gives

$$\mathscr{E}(x - x_0) = \pm\{[p_0 + \mathscr{E}z)^2 + (\chi^2/4)]^{1/2} - [p_0^2 + (\chi^2/4)]^{1/2}\},$$

that is, the trajectories of the rays are hyperbolas having the asymptotes x = ±z + const. The weakly absorbed rays are bent in the same direction as the reflecting planes, while the strongly absorbed rays are bent in the opposite direction. Here the curvature of the rays near the vertex of the hyperbola in the case of (5.14) exceeds the curvature of the reflecting planes by a factor of $2\tan^2\theta/\chi$, i.e., by 4—5 orders of magnitude.

A number of authors[25d,39] have studied experimentally the effect of curvature of x-rays in crystals undergoing elastic or thermal bending, and they have shown that the experimental data agree well with the theoretical predictions.

If the force $\mathscr{E}$ does not depend on z (e.g., the deformation field is planar, and it depends only on the coordinates x and y), then Eq. (5.9) implies conservation of the "energy" of (5.6) along the ray trajectories. In this case, the equation of the ray trajectory acquires the simple form

$$(dx/dz)^2 = 1 - \{\chi^2/4\,[H - (\alpha/4)]^2\}.$$

At the points $\alpha(x) = 4H \mp 2\chi$, which correspond to the turning points in the motion of a charged particle, the slope of the ray changes sign (it is "reflected"). Owing to such relfections, bands having elevated values of α(x) can serve as waveguides for the weakly absorbed rays, while bands having depressed values of α(x) will be waveguides for the strongly absorbed rays. In the case of the Borrmann effect, this leads to positive contrast in the regions having elevated values of α(x).

If a distorted region having some distribution of α(r) is small in comparison with the thickness of the crystal, then the rays deflected in this region will give rise to a shadow in the image surrounded by a brighter halo. Figure 13 illustrates such a case with the example of a dislocation parallel to the surface of the crystal (anomalous-transmission case, μt = 35; the numbers attached to the rays indicate the initial shape of the ray

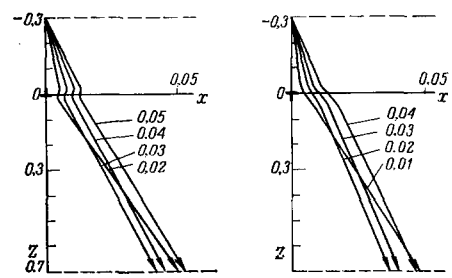

FIG. 13. Deviation of the rays of the weakly absorbed wave near edge dislocations. [40a]

FIG. 14. X-ray image of dislocations observed under anomalous-transmission conditions. [35]

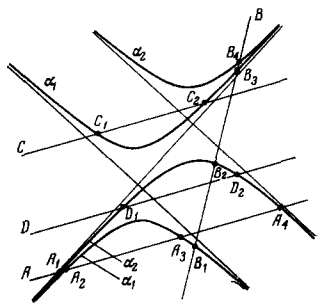

FIG. 15. Reflection and refraction of x-ray waves at an internal phase boundary between media having different values of the parameter α.

with respect to the z axis). The thickness of the specimen is assumed to be so great that one needs to account only for the weakly absorbed rays. Figure 14 shows a typical x-ray photograph of a crystal taken under conditions of anomalous transmission of x-rays. The regions of dislocations that are separated from the exit face by distances greater than the photoelectric-absorption distance are imaged in the form of shadows having a bright border, as is explaned by the course of the rays shown in Fig. 13 (cf. also Fig. 7b).

b) Reflection and refraction of x-rays. We cannot treat the study of the course of the rays in the case in which the parameter $\alpha(\mathbf{r})$ varies discontinuously as being the limiting case of trajectory curvature due to a concentrated force. This is because we must consider the possibility of immediate appearance at the phase boundary of two waves, which corresponds to splitting of the ray.

In order to derive the conditions for refraction and reflection of x-rays at an internal boundary separating regions having different values of the parameter $\alpha(\mathbf{r})$ (e.g., α_1 and α_2), let us compare the dispersion surfaces for these values of α (Fig. 15). The condition of continuity of the eikonal at the phase boundary implies, in analogy to the case of (2.10), that the discontinuities in the wave vectors of the reflected and refracted waves (as compared with that of the incident wave) occur only in the direction of the normal n to the phase boundary. Correspondingly, only those points on the dispersion surfaces can be excited that lie on a straight line parallel to n. In general, each such line intersects the dispersion surfaces having $\alpha = \alpha_1$ and $\alpha = \alpha_2$ in four points. One of these points corresponds to the given incident wave. Of the other three, one corresponds to a second possible incident wave, and two to actually appearing refracted waves (whenever the normal lies within the Borrmann delta) and reflected waves (if the normal lies outside the Borrmann delta). Both possible variants are illustrated in Fig. 15 by

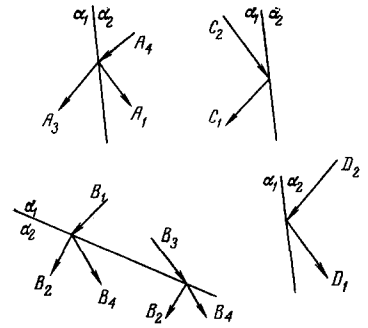

FIG. 16. Course of the rays upon passing through a phase boundary between two media.

cases A and B). When the straight line parallel to n intersects only one dispersion surface, total internal reflection occurs, and only one reflected wave arises. In contrast to light optics, total internal reflection can occur in x-ray optics on both sides of a phase boundary (cases C and D in Fig. 15). Figure 16 illustrates the course of the rays for all the cited cases. The numbering of the rays corresponds to the numbering of the points in Fig. 15, and the directions of the rays are parallel to the normals to the dispersion surfaces drawn at the corresponding points.

For a given orientation n of the phase boundary, the regions in which the different special cases of reflection and refraction of x-rays are realized are divided in phase diagrams like Fig. 15 by the tangents drawn parallel to the vector n (whenever the normal n lies outside the Borrmann delta), and by straight lines parallel to n passing through the vertices of the hyperbolas (whenever the normal lies within the Borrmann delta). In all cases, the points on the limiting lines correspond to merged directions of pairs of rays.

The relation between the amplitudes of the incident, reflected, and refracted waves at the phase boundary, which in ordinary optics is described by the Fresnel formulas, is established in x-ray optics by the condition of continuity of the electromagnetic field. In the E_0, E_1 plane, this corresponds to the condition that the vector sum of the amplitudes of the waves that arise at the phase boundary equals the vector amplitude of the incident wave. Since the relation between the amplitudes E_0 and E_1 for each wave is unequivocally fixed according to (2.11) by its wave vector, the problem is reduced to resolving the known vector amplitude of the incident wave into two components in the given directions.

As an example, let us consider reflection and refraction at a boundary perpendicular to the reflection vector ($\mathbf{n} \parallel \mathbf{K}_1$). In this case, only the P component of the wave vector shows a discontinuity at the phase boundary, while the H component is conserved. Let the incident ray have the positive slope

$$k = dx/dz = [P - (\alpha_1/4)]/[H - (\alpha_1/4)];$$

Then the reflected ray having $P_1 = (\alpha_1/2) - P$ has the negative slope $k_1 = -k$. For the refracted wave, Eq. (5.5) implies

$$P_2 = (\alpha_2/4) + \{[H - (\alpha_2/4)]^2 - (\chi/2)^2\}^{1/2} = (\alpha_2/4) + \{[(\alpha_1 - \alpha_2)/4) + (\chi/2)(1 - k^2)^{-1/2}]^2 - (\chi/2)^2\}^{1/2}. \quad (5.16)$$

When $H < (\alpha_2/4) - (\chi/2)$, a weakly absorbed wave arises, but when $H > (\chi/2) + (\alpha_2/4)$, a strongly absorbed refracted wave arises that has the positive slope

$$k_2 = \frac{P_2 - (\alpha_2/4)}{H - (\alpha_2/4)} = \{1 - [((\alpha_1 - \alpha_2)/2\chi) + (1 - k^2)^{-1/2}]^{-2}\}^{1/2}. \quad (5.17)$$

When $|H - (\alpha_2/4)| < \chi/2$, (5.16) gives a complex value for P_2. This corresponds to total internal reflection (the straight lines H = const. in Fig. 12b pass between the vertices of the hyperbolas $\alpha = \alpha_2$). As one moves away from the phase boundary, the wave field decays according to an exponential law with the exponent

$$\operatorname{Im} P_2 = \{(\chi/2)^2 - [((\alpha_1 - \alpha_2)/4) + (\chi/2)(1 - k^2)^{-1/2}]^2\}^{1/2}.$$

After we transform to dimensionless coordinates and the variables H and P, Eq. (2.11) gives the following expression for the ratio of the amplitudes E_0 and E_1 in each wave:

$$E_0/E_1 = \chi_{-1}C/2\,(P - H). \quad (5.18)$$

Let the amplitudes E_0 in the incident, reflected, and refracted waves be related as $1 : A_1 : A_2$. The condition of continuity of the wave field at the phase boundary gives

$$\begin{pmatrix} \chi_{-1}C/2 \\ P-H \end{pmatrix} + A_1 \begin{pmatrix} \chi_{-1}C/2 \\ P_1-H \end{pmatrix} = A_2 \begin{pmatrix} \chi_{-1}C/2 \\ P_2-H \end{pmatrix},$$

Hence,

$$A_1 = (P_2 - P)/(P_1 - P_2), \quad A_2 = (P_1 - P)/(P_1 - P_2). \quad (5.19)$$

Equations (5.16), (5.17), and (5.19) permit one to analyze fully the problem of reflection and refraction of x-rays for arbitrary values of the parameters k, α_1, and α_2.

Reflection and refraction of x-rays at internal boundaries that separate regions having different values of the parameters χ_1 and χ_{-1} (domains, twins, and in particular, inversion twins) can be reduced to the case treated above by joining the solutions together by the condition of continuity of the total wave field at the phase boundary.

6. IMAGE FORMATION IN TWO-RAY X-RAY OPTICS

Construction of the x-ray trajectories and their corresponding wave-vector trajectories allows one in principle to reconstruct the eikonals $S^{(I)}$ and $S^{(II)}$ for the two systems of rays and to proceed to determining the wave-field amplitudes $\hat{E}^{(I)}$ and $\hat{E}^{(II)}$. Since these amplitudes vary slowly, the intensity distribution in the x-ray image is initially determined by the difference between the eikonals $S^{(I)}$ and $S^{(II)}$, i.e., by the phase relations of the waves that correspond to the two systems of rays (pure phase contrast arises). With increasing depth in the crystal, the variation of the amplitudes $\hat{E}^{(I)}$ and $\hat{E}^{(II)}$ influence the intensity of the total field more and more. Finally, the strongly absorbed field practically vanishes, and it ceases to contribute to the x-ray image. Here the contrast does not depend on the value of the eikonal, and is determined by the amplitude of the weakly absorbed ray (pure amplitude contrast occurs).

The noted overall pattern of x-ray image formation becomes complicated if the rays belonging to one given system intersect and caustics arise. Then the determination of each wave field requires accounting for interference of all rays arriving at a given point. Thus, even when the strongly absorbed field completely vanishes, the image intensity continues to depend on the eikonal, which is a non-single-valued function of the coordinates.

a) Determination of the amplitudes of the wave field by the method of successive approximations. Using the general method,[20] we can seek the solution of Eq. (5.2) by successive approximations.[32] Let us assume for each wave field that

$$\hat{E} = \sum_{n=0}^{\infty} \hat{E}^{(n)}, \quad (6.1)$$

Here the zero-order-approximation term $\hat{E}^{(0)}$ satisfies the equation

$$D_S[\hat{E}^{(0)}] = 0, \quad (6.2)$$

while the subsequent terms satisfy the equation

$$D_S[\hat{E}^{(n+1)}] + D[\hat{E}^{(n)}] = 0. \quad (6.3)$$

Let us introduce the left-hand null vector $\hat{l} = (\chi_1 C/2, P - H)$ and the right-hand null vector $\hat{r} = (\chi_{-1}C/2, P - H)$ of the matrix D_S [the relation between the components of the vector $\hat{E}^{(0)}$ has been used above in (2.11) and (5.18)]. According to (6.2), the vector $\hat{E}^{(0)}$ can differ from $\hat{r}$ only by some scalar multiplier. If we assume that $\hat{E}^{(0)} = \sigma(x, z)\hat{r}$, and multiply Eq. (6.3) for n = 0 on the left-hand side by the vector $\hat{l}$, we get the "transport equation"

$$\hat{l}D[\sigma\hat{r}] = 0, \quad (6.4)$$

The latter permits us unambiguously to determine the variation in the field amplitude along the trajectory in the zero-order approximation if we know the initial values of E_0 and E_1 at the entrance surface of the crystal. Moreover, Eq. (6.3) permits us to determine in succession all the terms of the expansion in (6.1).

The "transport equation" (6.4) for the field amplitude in the zero-order approximation is fully equivalent to the law of conservation of energy flux of the wave field in a non-absorbing crystal, which was first derived by Kato[25c] and Kambe[40b]:

$$\operatorname{div} \mathbf{J} = 0, \quad \mathbf{J} = \varkappa E_0^2 + (\varkappa + \mathbf{K}_1) E_1^2.$$

The transport equation implies that the density of energy flux in the field corresponding to each of the eikonals $S^{(I)}$ and $S^{(II)}$ varies along the trajectories in inverse proportion to the distance between neighboring trajectories. In particular, in the case of anomalous transmission of x-rays, the image intensity in the undistorted regions of the crystal is determined substantially by the density of ray trajectories (see Fig. 13).

In the general case, considerable difficulties are now involved in carrying out the method of successive approximations of (6.1)–(6.3) with the eikonal chosen in the form (5.5), owing to the fact that we must account for the curvilinear nature of the rays. We can surmount this difficulty in weakly distorted crystals by choosing the eikonal in a form that corresponds to rectilinear rays. In particular, if we assume that $S = \pm i\chi z/2$, which corresponds to rays having

x = const., we get a system like (6.2) and (6.3) for the amplitudes $\hat{E}^{(n)}$, where, in contrast to (5.3) and (5.4),

$$D_S = \begin{pmatrix} \pm\chi/2 & \chi_{-1}C \\ \chi_1 C & \pm\chi/2 \end{pmatrix},$$

$$D = \begin{pmatrix} \frac{\partial}{\partial z}+\frac{\partial}{\partial x} & 0 \\ 0 & \frac{\partial}{\partial z}-\frac{\partial}{\partial x}+\frac{i\alpha}{2} \end{pmatrix}.$$

The transport equation (6.4) takes on the simple form

$$\left(\frac{\partial}{\partial z}+i\,\frac{\alpha}{4}\right)\sigma = 0,$$

Hence,

$$\hat{E}^{(0)} = 0{,}5\ (\mp\chi_{-1}C/\chi)\ \exp\left[-\left(\frac{i}{4}\right)\int_0^z \alpha\,(x,\,z)\,dz\right]. \qquad (6.5)$$

The next term of the series in (6.1) was also calculated in[32] for the case $\alpha = \alpha(x)$:

$$\hat{E}^{(1)} = e^{-i\alpha z/2}\left[-\frac{i}{4\chi}P_1(\alpha,\,z)\begin{pmatrix}1\\ \pm 1\end{pmatrix} - \frac{1}{\chi}\begin{pmatrix}\pm 1\\ 0\end{pmatrix}P_2(\alpha,\,z)\right], \qquad (6.6)$$

where

$$P_1(\alpha,\,z) = (\alpha^2 z/8) + \alpha'_x z\,[(\alpha z/8) + (\alpha'_x z^2/24) + i] + (i\alpha''_{xx}z^2/4),$$
$$P_2(\alpha,\,z) = (\alpha + \alpha'_x z)/2 \qquad (6.7)$$

(For simplicity we have taken $C = 1$, $\chi_1 = \chi_{-1} = -\chi$.) Equations (6.5)—(6.7) permit one to calculate explicitly the image contrast for any smooth function $\alpha(x, y)$ that varies little over distances of the order of the thickness of the crystal. Use of these formulas to calculate the image of an edge dislocation perpendicular to the surface of the crystal showed satisfactory agreement with the results of numerical solution of Takagi's equation (see Fig. 9c), and qualitative agreement of the calculated intensity distribution with x-ray photographs of dislocations.[33]

b) Asymptotic solution for the x-ray wave field in crystals having a two-dimensional distortion field. The case $\alpha = \alpha(x, y)$ involves considerable difficulty in constructing the wave field by methods of geometric optics, owing to the continuous increase in phase difference in adjacent regions of the crystal and the appearance of waveguide effects like those mentioned at the end of Sec. a of Chap. 5. On the other hand, when $\alpha = \alpha(x, y)$, the coefficients in Takagi's equation (4.2) do not depend on the variable z. This permits us to seek the solution of this equation by using integral transformations with respect to this variable. In order to study the asymptotic behavior of the wave field in thick crystals, a Laplace transformation was used in[41] that establishes a correspondence between the sought functions $E_0(x, z)$ and $E_1(x, z)$ and their images $F_0(x, p)$ and $F_1(x, p)$ according to the rules

$$\hat{F}(x,\,p) = \int_0^\infty e^{-pz}\hat{E}(x,\,z)\,dz$$

or in abbreviated notation, $\hat{E}(x, z) \div \hat{F}(x, p)$. This implies that the derivatives with respect to x and z are, respectively:

$$\frac{\partial\hat{E}(x,\,z)}{\partial x} \div \frac{\partial F(x,\,p)}{\partial x}, \quad \frac{\partial\hat{E}(x,\,z)}{\partial z} \div p\hat{F}(x,\,p) - \hat{E}(x,\,0).$$

Upon transforming to the functions F_0 and F_1, Takagi's equation is reduced to a system of ordinary first-order differential equations

$$\begin{pmatrix} 2i\left(p+\frac{\partial}{\partial x}\right) & \chi_{-1}C \\ \chi_1 C & 2i\left(p-\frac{\partial}{\partial x}\right)-\alpha(x) \end{pmatrix}\hat{F} = 2i\hat{E}(x,\,0), \qquad (6.8)$$

They are equivalent to the ordinary second-order differential equations for F_0 and F_1. Thus we have for the field of the diffracted wave:

$$\frac{\partial^2 F_1}{\partial x^2} - \frac{i\alpha}{2}pF_1 - \frac{i}{2}\frac{\partial\alpha F_1}{\partial x} - \left(p^2+\frac{\chi^2}{4}\right)F_1 = -\frac{i\chi_1 C}{2}E_0(x,\,0) - pE_1(x,\,0). \qquad (6.9)$$

Using the inverse Laplace transform

$$\hat{E}(x,\,z) = (1/2\pi i)\int_{p_0-i\infty}^{p_0+i\infty} e^{pz}\hat{F}(x,\,p)\,dp,$$

(where p_0 lies to the right of all singular points of $\hat{F}(x, p)$) to solve the system of (6.8) gives the sought wave field. The asymptotic behavior of the wave field at large values of z is determined by the behavior of the functions F_0 and F_1 near the singular points closest to the line of integration.

As an example, the image of a bicrystal was studied in[41] in which $\alpha(x, y) = \alpha(y)\,\theta(-x)$. In this case, under uniform illumination of the specimen ($E_0(x, 0) = 1$, $E_1(x, 0) = 0$), Eq. (6.9) for the diffracted wave takes on the form

$$F''_{xx} - (i\alpha/2)\,\theta(-x),$$
$$F'_x - [p^2 + i\,(\alpha/2)\,\theta(-x)\,p + (\chi^2/4) - (\alpha/2)\,\delta(x)]\,F = -i\chi/2.$$

The solution of this equation that satisfies the condition of being bounded at infinity has the form

$$F(x,\,p) = (i\chi/2)\,\{[p^2 + (\chi/2)^2 + ip\,(\alpha/2)\,\theta(-x)]^{-1} \cdot$$
$$\cdot\exp\left[i\,(\alpha/4)\,x\theta(-x) - |x|\,\{[p + i\,(\alpha/4)\,\theta(-x)]^2 + (\chi^2/4)\}^{1/2}\right]$$
$$\times\,([p^2 + (\chi/2)^2 + ip\,(\alpha/2)\,\theta(-x)]^{-1} +$$
$$+\,[p^2 + (\chi/2)^2]^{-1}\,[i\,(\alpha/4) - \{[p + i\,(\alpha/4)]^2 + (\chi^2/4)\}^{1/2}]^{-1})\}. \qquad (6.10)$$

One cannot perform the inverse Laplace transformation for the image of (6.10) in explicit form. However, we can elucidate all the characteristic features of the wave field by using the corresponding asymptotic solutions. For this purpose, a method was developed in this study of finding the asymptotic behavior of an original that resembles the ordinary method of expanding an image in a power series in the vicinity of singular points (see, e.g.[42]). The analysis was made for a non-absorbing crystal, which is the most difficult case for calculation, because here one must take into account all of the singular points $F(x, p)$ in the plane of the complex variable p. It was assumed for concreteness that $\alpha > 0$. We see from (6.10) that $F(x, p)$ has simple poles at $p = \pm i\chi/2$ and $p = -i(\alpha/4) \pm i[\chi^2/4) + (\alpha^2/16)]^{1/2}$, and branch points at $p = \pm i\chi/2$ and $p = -i(\alpha/4) \pm i(\chi/2)$. The real part of all the singular points is zero (non-absorbing crystal). Hence they are all essential in the asymptotic behavior of the original When $|\alpha| \ll \chi$, $|\alpha z| \gg 1$, and $|x| \ll z/(\chi z)^{1/4}$, the field of the diffracted wave has the form

$$E_1(x,\,z) \approx i\,\mathrm{Im}\,[e^{i\chi z/2}\Phi(x\,(i\chi/4z)^{1/2})],\quad x > 0,$$
$$E_1(x,\,z) \approx (i/2)\,e^{-i\alpha z/2}\,(1 - e^{i\alpha x/2})\sin[(\chi z/2) + (\alpha^2 z/16\chi)] +$$
$$+\,(i/2)\,e^{-i\alpha z/2}\,\mathrm{Im}\,\{e^{iz[(\chi/2)+(\alpha^2/16\chi)]}\,\Phi((i\alpha^2 z/16\chi)^{1/2} - (i\chi/4z)^{1/2}\,x)\}$$
$$-\,(i/2)\,e^{-i(\alpha/4)x+i(\alpha/2)x}\,\mathrm{Im}\,\{e^{iz[(\chi/2)+(\alpha^2/16\chi)]}\Phi((i\alpha^2 z/16\chi)^{1/2}$$
$$+\,(i\chi/4z)^{1/2}\,x)\},\quad x < 0, \qquad (6.11)$$

where $\Phi(t)$ is the probability integral.

According to (6.11), the intensity $I_1(x, z)$ in the

region $x > 0$ increases according to a parabolic law over the segment $0 \leq x \lesssim z/(\chi z/4)^{1/2}$. Thenceforth it oscillates with declining amplitude, and approaches a value corresponding to the solution of (2.14) for $\alpha = 0$. In the region $x < 0$ and $\alpha^2 z/16\chi \ll 1$, the intensity oscillates over the segment $-\alpha z/2\chi \lesssim x \lesssim 0$ with an amplitude of the order of unity, and then it approaches a value corresponding to the solution of (2.14) with $\alpha \neq 0$.

For a highly disoriented bicrystal in which $|\chi| \ll \alpha$, the asymptotic solution for the region $\alpha z \gg 1$ has the following form: in the region $x \leq -z$, it is the ordinary solution of (2.14) for $\alpha \neq 0$; in the region $0 \leq (x + z)\alpha/4 \leq 1$, we have

$$E_1(x, z) \approx (2\chi/\alpha)(1 - e^{-i\alpha z/4}) - (\alpha\chi/8)(x + z)^2 e^{-i\alpha z/2},$$

and in the region $(x + z)\alpha/4 \gg 1$ when $x < 0$,

$$E_1(x, z) \approx (i\chi/2)(z + x) e^{i\alpha x/2} \{J_0(\chi(z + x)/2) + (\pi/2)[J_1(\chi(z+x)/2) \times \mathbf{H}_0(\chi(z + x)/2) - J_0(\chi(z + x)/2)\mathbf{H}_1(\chi(z + x)/2)]\}, \quad (6.12)$$

where $\mathbf{H}_\nu(t)$ is a Struve function. In particular,

$$E_1(x, z) = \begin{cases} i(\chi/2)(z+x) e^{i\alpha x/2}, & \chi(z+x) \ll 1, \\ ie^{i\alpha x/2}, & \chi(z+x) \gg 1. \end{cases} \quad (6.13)$$

In line with (6.12) and (6.13), the intensity for $x < 0$ hardly oscillates, but remains of a size near unity over the interval $(-z + (2/\chi), 0)$ and declines along a parabola over the range $(-z + (4/\alpha), -z + (2/\chi))$.

In the region $0 < x \leq z/(\chi z)^{1/4}$, the asymptotic behavior of $E_1(x, z)$ has this form:

$$E_1(x, z) = i\sqrt{2}\{\sin[(\chi(z/2) + (\pi/4)] C(x^2\chi/4z) - \cos[(\chi z/2) + (\pi/4)] S(x^2\chi/4z)\} + \{i\alpha\chi \exp[-i(\alpha/4)z + iz[(\alpha^2/16) + (\chi^2/4)]^{1/2} - x\{(\alpha/2)[(\alpha^2/16) + (\chi^2/4)]^{1/2} - (\alpha^2/8)\}^{1/2}] \times \{2(\alpha^2 + 4\chi^2)^{1/2}[(\alpha/2)[(\alpha^2/16) + (\chi^2/4)]^{1/2} - (\alpha^2/8)]^{1/2}\}^{-1}, \quad (6.14)$$

where $C(t)$ and $S(t)$ are Fresnel functions. Eq. (6.14) also holds when $\alpha \sim \chi$ and $x > 0$. When $\alpha \gtrsim \chi$ in the region $x > 0$, the intensity of the x-ray image declines exponentially over the segment $0 \leq x\chi/2 \lesssim 1$ (total internal reflection!). Then it increases along a parabola over the region $(2/\chi, z/(\chi/2)^{1/2}$. Beyond, it oscillates with declining amplitude and approaches a value corresponding to the solution of (2.14) with $\alpha = 0$. The study conducted in[41] shows that the deviations from geometric optics are substantial only in the regions $\chi(z + x)/2 \ll 1$ and $1 \lesssim (\chi z)^{1/2}$, even under conditions of total internal reflection.

7. CONCLUSION

The theory of x-ray images has taken only the first steps as compared with that of electron-microscopic diffraction images. A number of the ways of analyzing images that are used in electron microscopy have as yet no analogy in x-ray topography. The variety of possible cases and the awkwardness of the numerical methods of image calculation have hindered compilation of atlases of images of typical lattice defects. However, most of the problems allow effective qualitative and even quantitative study to solve the problem of image analysis in practical cases.

The scattering of radiation from regions having local distortions is represented well by the Green's functions: analysis of the conditions for appearance and decay of the Bloch waves of the first and second types determines the conditions for appearance and disappearance of extinction fringes; and the path of the x-rays in weakly distorted crystals is amenable to simple estimates, including reflection and refraction of rays at inner boundaries. The worse difficulties arise in analyzing the images of distortion fields that extend along the reflecting planes. Then caustics can easily arise, and waveguide effects, total internal reflection effects, and other such phenomena can arise and interfere with use of geometrical optics. In such a case, the most promising thing to do is to use asymptotic methods of studying the wave field.

A single approach to analyzing x-ray images seems impossible. Highly varied methods may prove effective, depending on the concrete problem. We can hope that the arsenal of methods of x-ray topography will be expanded further in the course of experimental testing of the above-cited methods of image analysis. In particular, it is of interest to test the qualitative predictions of the connection between the sign of the contrast and simple characteristics of distortion fields, and to test quantitatively the expressions that express explicitly the images of weakly distorted regions of a crystal and the theoretical conclusions on the images of local distortions of the Green's functions and on the form of the initial perturbations of the wave field in strongly distorted regions. It is also of interest to make a quantitative study of images for special defect positions, to perform interferometry of distortion fields using sectional topograms and Fourier analysis of the latter, to study extinction effects in images obtained under anomalous x-ray transmission conditions, to test quantitatively the theory of x-ray refraction and reflection at inner boundaries, to study waveguide and total internal reflection effects, and to construct x-ray-optical devices resembling Fresnel lenses and various dislocation lenses. We can hope that, as we make progress in understanding the mechanisms of these phenomena, a transition will begin from passively studying various phenomena that complicate analysis of x-ray images to consciously using them in various x-ray optical instruments.

A number of problems of the theory of x-ray images that took no part in this review are also worth mentioning. These include image analysis in reflected beams (in Bragg diffraction)*, the x-ray moiré effect, accounting for angular divergence and incoherence of the radiation incident on the crystal, and analysis of the contribution of thermal vibrations and diffuse scattering.

In conclusion, we thank deeply Z. G. Pinsker, I. L. Shul'pina, and V. I. Nikitenko, whose advice and suggestions stimulated writing this article.

[1] G. S. Zhdanov, Osnovy rentgenovskogo strukturnogo analiza (Fundaments of x-ray Structure Analysis), Gostekhizdat, M.-L., 1940; A. I. Kitaĭgorodskiĭ,

*Recently published studies [27] have made substantial progress in solving the spatially-inhomogeneous problem of Bragg diffraction. In particular, the Green's functions were derived in these studies for a point source, and expressions were derived for the wave field in the crystal [cf. (3.8) and (3.9)] with the boundary condition $E_1(x, z)_{z=t} = 0$ for a z value equal to the thickness t of the specimen.

Rentgenostrukturnyĭ analiz (X-ray Structure Analysis), Gostekhizdat, M., 1950 (Engl. Transl., The Theory of Crystal structure Analysis, Consultants Bureau, N. Y., 1961).

[2]M. A. Krivoglaz, Teoriya rasseyaniya rentgenovskikh lucheĭ i teplovykh neĭtronov realnymi kristallami (Theory of X-ray and Thermal-neutron Scattering by Real Crystals), Nauka, M., 1967, Part I (Engl. Transl., Plenum Press, N. Y., 1969).

[3]A. Guinier, Theorie et technique de la radiocristallographie, Dunod, Paris, 2nd Ed., 1956; 3rd Ed., 1964, Part 4, Chap. 8, Sec. 3 (Engl. Transl., 1st Ed., Hilger + Watts, London, 1952; Russ. Transl., Fizmatgiz M., 1961); D. M. Vasil'ev and B. I. Smirnov, Usp. Fiz. Nauk **73**, 503 (1961) [Sov. Phys.-Uspekhi **4**, 226 (1961)].

[4]M. A. Blokhin, Fizika rentgenovskikh lucheĭ (Physics of X-rays), 2nd Ed., Gostekhizdat, M., 1957, pp. 8–10.

[5]W. A. Wooster, Diffuse X-ray Reflections from Crystals, Clarendon Press, Oxford, 1962, Chap. II (Russ. Transl., IL, M., 1963).

[6]C. G. Darwin, Phil. Mag. **27**, 315, 675 (1914); P. P. Ewald, Ann. Physik **54**, 519 (1917); Z. Physik **2**, 332 (1920); **30**, 1 (1924).

[7]S. Amelinckx, The Direct Observation of Dislocations (Solid State Physics, Suppl. 6), Academic Press, N. Y., 1964; G. Hildebrandt, Reinstoffprobleme Ed. E. Rexer, Akademie-Verlag, B., 1967, p. 151.

[8]A. M. Elistratov, concluding remarks in: Pryamye metody issledovaniya defektov v kristallakh (Direct Methods of Studying Defects in Crystals), Mir, M., 1965, p. 268.

[9]A. Authier, a) Adv. X-ray Anal. **10**, 9 (1967); b) Phys. Stat. Sol. **27**, 77 (1968).

[10]G. Borrmann, a) Z. Physik **42**, 157 (1941); **127**, 197 (1950); Beiträge zur Chemie und Physik des 20. Jahrhunderts—Lise Meitner, Otto Hahn, Max von Laue zum 80. Geburtstag, Ed. O. R. Frisch, et al., F. Vieweg und Sohn, Braunschweig, 1959, p. 262; b) Phys. Blätter **11**, 508 (1959).

[11]O. N. Efimov and A. M. Elistratov, Fiz. Tverd. Tela **4**, 2908 (1962) [Sov. Phys.-Solid State **4**, 2131 (1963).

[12]A. M. Afanas'ev and Yu. Kagan, Zh. Eksp. Teor. Fiz. **52**, 191 (1967) [Sov. Phys.-JETP **25**, 124 (1967)]; Acta Cryst. **A24**, 163 (1968).

[13]E. A. Tikhonova, Fiz. Tverd. Tela **9**, 516 (1967) [Sov. Phys.-Solid State **9**, 394 (1967)]; A. M. Afanas'ev, Yu. Kagan, and F. N. Chukhovskiĭ, Dynamical Treatment of the X-ray Thermal Diffuse Scattering, I. V. Kurchatov Institute of Atomic Energy Preprint IAÉ-1476, Moscow, 1967; A. M. Afanasev, Yu. Kagan, and F. N. Chukhovskiĭ, Phys. Stat. Sol. **28**, 287 (1968).

[14]A. J. W. Sommerfeld, Vorlesungen über theoretische Physik, Vol. 4. Optik, Akad. Verlagsgesell. Geest + Portig, 1950 (Engl. Transl., Acad. Press, 1964; Russ. Transl., IL, M., 1953).

[15]L. G. Orlov, M. P. Usikov, and L. M. Utevskiĭ, Usp. Fiz. Nauk **76**, 109 (1962) [Sov. Phys.-Uspekhi **5**, 53 (1962)]; V. N. Rozhanskiĭ, Zav. lab. **32**, 170 (1962).

[16]P. B. Hirsch, et al., Electron Microscopy of Thin Crystals, Butterworths, L., 1965, Chap. 11 (Russ. Transl., Mir, M., 1968).

[17]J. M. Ziman, Principles of the Theory of Solids, University Press, Cambridge, 1964, Chap. 3 (Russ. Transl., Mir, M., 1966).

[18]M. von Laue, a) Acta Cryst. **2**, 106 (1949); **5**, 619 (1952); b) Röntgenstrahl-interferenzen, 3. Aufl., Akademische Verlagsges., Frankfurt am Main, 1960; W. H. Zachariasen, Theory of x-ray Diffraction in Crystals, Wiley, N. Y., 1945; W. Batterman and H. Cole, Rev. Mod. Phys. **36**, 681 (1964).

[19]A. Authier and A. R. Lang, J. Appl. Phys. **35**, 1956 (1964).

[20]R. Courant, Partial Differential Equations, Chap. V, Sec. 5, (Russ. Transl., "Mir", M., 1964).

[21]I. Sh. Slobodetskiĭ, F. N. Chukhovskiĭ, and V. L. Indenbom, ZhÉTF Pis. Red. **8**, 90 (1968) [JETP Lett. **8**, 55 (1968)].

[22]I. Sh. Slobodetskiĭ and F. N. Chukhovskiĭ, Kristallografiya **15**, 1101 (1970) [Sov. Phys.-Crystallogr. **15**, 963 (1971)].

[23]É. V. Suvorov, V. I. Polovinkina, and V. I. Nikitenko, Fiz. Tverd. Tela **13**, 2692 (1971) [Sov. Phys.-Solid State **13**, 2253 (1972)].

[24]M. Hart and A. D. Milne, Acta Cryst. **A25**, 134 (1969); **A26**, 223 (1970).

[25]N. Kato, Acta Cryst. a) **14**, 526, 627 (1961); b) ibid. **A25**, 119 (1969); c) J. Phys. Soc. Japan, **18**, 1785 (1963); **19**, 67 (1964); d) ibid. **19**, 971 (1964); e) ibid. **20**, 1047 (1965); **21**, 160, 1772 (1966); f) J. Appl. Phys. **39**, 2225, 2231 (1968).

[26]A. Authier and D. Simon, Acta Cryst. **A24**, 517 (1968).

[27]A. M. Afanas'ev and V. G. Kon, a) Dinamicheskaya teoriya rentgenovskikh lucheĭ v kristallakh s defektami (Dynamical Theory of X-rays in Crystals with Defects). Preprint of the I. V. Kurchatov Institute of Atomic Energy IAÉ-1890, 1969; b) A. M. Afanas'ev and V. G. Kohn, Acta Cryst. **A27**, 421 (1971); T. Uragami, J. Phys. Soc. Japan **27**, 147 (1969); **28**, 1508 (1970).

[28]F. Balibar and A. Authier, Phys. Stat. Sol. **21**, 413 (1967).

[29]S. Takagi, a) Acta Cryst. **15**, 1311 (1962); b) J. Phys. Soc. Japan **26**, 1239 (1969).

[30]D. Taupin, Bull. Soc. Fr. Miner. Cryst. **87**, 469 (1964); Acta Cryst. **23**, 25 (1967).

[31]A. Authier, C. Malgrange, and M. Tournarie, Acta Cryst. **A24**, 126 (1968).

[32]F. N. Chukhovskii and A. A. Shtolberg, Phys. Stat. Sol. **41**, 815 (1970).

[33]V. F. Miuskov and P. S. Milevskiĭ, Izv. Akad. Nauk SSSR (*Neorganicheskie materialy*) **1**, 1267 (1965).

[34]A. K. Head, Austr. J. Phys. **20**, 557 (1967); P. Humble, ibid. **21**, 325 (1968); A. R. Thölen, Phil. Mag. **22**, 175 (1970).

[35]I. L. Shul'pina, Candidate's dissertation (IP AN SSSR, Leningrad, 1968).

[36]A. R. Lang, Acta Cryst. **12**, 249 (1959); J. Appl. Phys. **30**, 1748 (1959); Z. Naturforsch. **20a**, 636 (1965).

[37]N. Kato and Y. Ando, J. Phys. Soc. Japan **21**, 964 (1966); J. R. Patel and N. Kato, Appl. Phys. Lett. **13**, 40 (1968).

[38]L. D. Landau and E. M. Lifshits, Teoriya polya (Field Theory), Nauka, M., 1967, Sec. 17 (Engl. Transl., The Classical Theory of Fields, Pergamon Press, N. Y., 1971).

[39]P. Penning and D. Polder, Philips Res. Rept. **16**,

499 (1961); B. Okkerse and P. Penning, ibid. 18, 82 (1963); H. Cole and G. E. Brock, Phys. Rev. 116, 268 (1959).

[40] K. Kambe, Z. Naturforsch. a) 18a, 1010 (1963); b) 20a, 770 (1965).

[41] G. N. Dubnova, V. L. Indenbom, S. A. Pikin, and F. N. Chukhovskiĭ, Kristallografiya 16, 18 (1971) [Sov. Phys.-Crystallogr. 16, 9 (1971)].

[42] G. Doetsch, Anleitung zum praktischen Gebrauch der Laplace-Transformation, R. Oldenbourg, München, 1956, Secs. 34–35 (Engl. Transl., Van Nostrand, N. Y., 1961; Russ. Transl., Nauka, M., 1971).

Translated by M. V. King